nature cancer

Article

https://doi.org/10.1038/s43018-023-00525-y

Age-associated microenvironmental changes highlight the role of PDGF-C in ER$^+$ breast cancer metastatic relapse

Received: 18 March 2022

Accepted: 7 February 2023

Published online: 13 March 2023

Check for updates

Frances K. Turrell[1], Rebecca Orha[1], Naomi J. Guppy[2], Andrea Gillespie[1], Matthew Guelbert[3], Chris Starling[2], Syed Haider[1] & Clare M. Isacke[1]

Patients with estrogen receptor (ER)-positive breast cancer are at risk of metastatic relapse for decades after primary tumor resection and treatment, a consequence of dormant disseminated tumor cells (DTCs) reawakening at secondary sites. Here we use syngeneic ER$^+$ mouse models in which DTCs display a dormant phenotype in young mice but accelerated metastatic outgrowth in an aged or fibrotic microenvironment. In young mice, low-level *Pdgfc* expression by ER$^+$ DTCs is required for their maintenance in secondary sites but is insufficient to support development of macrometastases. By contrast, the platelet-derived growth factor (PDGF)-C^{hi} environment of aging or fibrotic lungs promotes DTC proliferation and upregulates tumor cell *Pdgfc* expression stimulating further stromal activation, events that can be blocked by pharmacological inhibition of PDGFRα or with a PDGF-C-blocking antibody. These results highlight the role of the changing microenvironment in regulating DTC outgrowth and the opportunity to target PDGF-C signaling to limit metastatic relapse in ER$^+$ breast cancer.

Metastasis remains the cause of nearly all breast cancer-related deaths. ER$^-$ breast cancers have poorer prognosis, with disease recurrence typically occurring within 5 years[1]. Conversely, although they have a better prognosis initially, patients with ER$^+$ disease have a substantial risk of late recurrence and may present with metastatic disease decades later[1,2]. Underlying this extended latency period is the ability of ER$^+$ DTCs to survive at the secondary site in a quiescent therapy-resistant state until triggered to re-enter proliferation and form clinically detectable metastatic lesions. The secondary-site microenvironment is key to controlling both tumor cell survival and subsequent exit from dormancy[3–11]. However, mechanistic understanding of the microenvironmental cues controlling recurrence remains limited due to the absence of suitable preclinical models of ER$^+$ metastatic relapse, with the majority of studies using ER$^+$ human breast cancer cells in immunocompromised mice or ER$^-$ mouse mammary tumor cells. Further, given the longer latency of ER$^+$ late recurrence, it is crucial to investigate metastatic relapse in models of the aging microenvironment.

In this study, we have characterized and used syngeneic models of ER$^+$ breast cancer to demonstrate how microenvironmental changes due to aging or fibrotic injury support proliferation and outgrowth of DTCs. From transcriptional profiling, we identity *Pdgfc* as a key factor upregulated in aged and fibrotic lungs, associated with an accumulation of activated fibroblasts and enhanced metastatic outgrowth. By contrast, in the PDGF-C^{lo} microenvironment of young mice, expression of *Pdgfc* by disseminated ER$^+$ tumor cells is required for DTC survival, highlighting the opportunity of targeting PDGF-C signaling to limit ER$^+$ breast cancer recurrence.

Results

Syngeneic models of ER$^+$ breast cancer metastatic relapse

To investigate the mechanisms controlling ER$^+$ breast cancer relapse, we characterized four mouse mammary tumor cell lines reported to be ER$^+$ (ref. [12]). RNA sequencing (RNA-seq) confirmed, as previously reported[12], that EMT6 cells exhibit a claudin-low, mesenchymal phenotype,

[1]The Breast Cancer Now Toby Robins Research Centre, The Institute of Cancer Research, London, UK. [2]The Breast Cancer Now Toby Robins Research Centre Nina Barough Pathology Core Facility, The Institute of Cancer Research, London, UK. [3]Flow Cytometry Facility, Chester Beatty Laboratories, The Institute of Cancer Research, London, UK. e-mail: clare.isacke@icr.ac.uk

whereas claudin-expressing TSAE1, HRM1 and F3II cells display an epithelial morphology (Extended Data Fig. 1a,b). TSAE1, HRM1 and EMT6 cell lines had high *Esr1* expression, but F3II cells expressed levels comparable to those of the ER$^-$ D2A1 line and metastatic derivatives D2A1-m1 and D2A1-m2 (ref. [13]) (Fig. 1a and Extended Data Fig. 1c). ER signaling pathway genes were upregulated in TSAE1, HRM1 and EMT6 cells compared to ER$^-$ cell lines, while 4-hydroxytamoxifen (4-OHT) treatment reduced expression of the ER response gene *Greb1* (Fig. 1b,c and Extended Data Fig. 1d). Similarly, the enhanced colony growth of TSAE1 and HRM1 cells in estrogen-containing medium was impaired by both 4-OHT and the selective ER degrader fulvestrant (Fig. 1d and Extended Data Fig. 1e). When grown as orthotopic tumors in syngeneic immunocompetent mice, TSAE1, HRM1 and EMT6 cells formed ER$^+$ mammary tumors (Fig. 1e). Implantation of mice with estradiol pellets augmented growth of TSAE1 and, to a lesser extent, HRM1 tumors (Fig. 1f and Extended Data Fig. 1f); however, all three ER$^+$ lines formed mammary tumors in mice without estrogen supplementation, hence better recapitulating the lower estradiol levels in older women.

In standard two-dimensional culture, the mouse ER$^+$ lines grew comparably to the ER$^-$ 4T1 and D2A1 lines (Extended Data Fig. 2a) but displayed a non-proliferative phenotype, remaining as single cells or small cell clusters when cultured in reduced-serum medium for 7–10 d; however, these cells could be stimulated to re-enter proliferation by subsequent culture in conditioned medium (CM) from ER$^-$ 4T1 cells or normal lung fibroblasts (Extended Data Fig. 2b,c). Comparable results were observed with ZR-75-1 human ER$^+$ breast cancer cells, with release from dormancy enhanced with cancer-associated fibroblast (CAF) CM compared to normal fibroblast CM (Extended Data Fig. 2d). Similarly, ER$^+$ but not ER$^-$ lines displayed a dormant phenotype when cultured in soft agar for 6 weeks or in growth factor-reduced basement membrane extract (BME)[4] for 9–15 d, with cells demonstrating retention of the lipophilic dye DiD (Extended Data Fig. 2e–g). When the ER$^+$ lines were injected orthotopically into syngeneic mice without supplemental estrogen, the experiment ended due to the primary tumors reaching maximum allowable size, with no evidence of ill health caused by metastatic disease. Indeed, subsequent histopathology revealed only small numbers of metastatic deposits in the lungs of some mice. By contrast, all mice bearing 4T1 tumors reached endpoint due to metastatic burden (Fig. 1g). To detect single DTCs in lungs, TSAE1, HRM1 and EMT6 cells were engineered to express mCherry and luciferase (mChLuc2). Following orthotopic implantation, organs were imaged with the In Vivo Imaging System (IVIS) ex vivo when tumors reached a size comparable to that of 4T1 tumors that cause symptomatic metastatic disease (~700–1,000 mm^3). A positive IVIS signal was detected; however, immunostaining for luciferase revealed only single DTCs or small clusters (typically <10 cells), with no detectable macrometastatic disease in the lungs (Fig. 1h) or other organs (Extended Data Fig. 2h). Given the high ER expression and luminal classification, we focused on the TSAE1-BALB/c model, using the HRM1-FVB model for validation. No further experiments were performed with the EMT6 line due its non-epithelial, claudin-low phenotype.

An aged microenvironment promotes outgrowth of ER$^+$ DTCs

Given the longer latency preceding ER$^+$ distant recurrence, we sought to establish whether an aging microenvironment could promote outgrowth of ER$^+$ DTCs. TSAE1 primary tumors grew comparably irrespective of mouse age, but only single DTCs or small tumor cell clusters were present in the lungs from young (12 weeks at endpoint) mice, whereas lungs from aged mice (16 months at endpoint) showed a significantly increased metastatic burden (Fig. 2a and Extended Data Fig. 3a). Labeling with 5-ethynyl-2′-deoxyuridine (EdU) confirmed that only a small percent of tumor cells in young lungs were proliferative, but a dramatically higher number of proliferating (EdU$^+$) tumor cells were found in both small clusters and large metastatic deposits in aged lungs (Fig. 2b and Extended Data Fig. 3b). Using an experimental (intravenous tumor cell-inoculation) metastasis model, metastatic burden in all mice was greater than that observed in spontaneous models, likely due to the higher number of DTCs seeding in the lungs, albeit with metastatic lesions in young mice largely restricted to the lung edge and bronchial tree, while aged mice displayed a higher metastatic burden and a wider distribution of metastases with prominent lesions in the lung parenchyma (Fig. 2c and Extended Data Fig. 3c).

RNA-seq profiles of lungs from naive young and aged BALB/c mice clustered based on age, with fibroblast activation and fibrosis genes differentially expressed (Fig. 2d and Extended Data Fig. 3d). To model lung fibrosis, we used intranasal bleomycin treatment, which promotes fibroblast activation, macrophage infiltration and enhanced collagen deposition (Extended Data Fig. 3e). Following either intravenous or orthotopic inoculation, ER$^+$ TSAE1 cells showed significantly enhanced metastatic outgrowth in bleomycin-treated lungs (Fig. 2e,f), again with a notable increase in macrometastases within the lung parenchyma. Given these findings and the striking reactivation of tumor cell proliferation by fibroblast CM in our in vitro dormancy models (Extended Data Fig. 2b–d), we focused on pro-fibrotic factors that may support metastatic outgrowth in aged mice. It was intriguing to observe divergent patterns of expression of PDGF family members in the RNA-seq data, with lower expression of classical PDGFs, *Pdgfa* and *Pdgfb*, in aged mouse lungs compared to elevated expression of *Pdgfc* and *Pdgfd* (Fig. 2g). Additionally, *Pdgfc* expression and levels of PDGF-C protein were significantly upregulated in fibrotic lungs following bleomycin treatment, whereas expression of other PDGF family members was significantly downregulated (Fig. 2h and Extended Data Fig. 3f,g). These findings were validated by analysis of an independent RNA-profiling dataset of lungs from bleomycin-treated C57BL/6 mice[14] (Extended Data Fig. 4a). In addition, in human lung tissue collected from 1,197 patients between 4 and 85 years of age[15] expression

Fig. 1 | Mouse models of ER$^+$ breast cancer metastatic relapse. a,**b**, RNA-seq analysis of mouse mammary tumor cell lines. **a**, *Esr1* expression. **b**, Left, heatmap showing significantly differentially expressed genes ($|\log_2$ (fold change)$| > 0.585$, P value < 0.05) between ER$^-$ (F3II, D2A1, D2A1-m1, D2A1-m2) and ER$^+$ (TSAE1, HRM1, EMT6) lines. Right, Ingenuity Pathway Analysis showing the top four significantly ($P < 0.05$, right-tailed Fisher's exact test) upregulated pathways (ER$^+$ versus ER$^-$ lines). Dashed line, P value cutoff. CLEAR, coordinated lysosomal expression and regulation. **c**, *Greb1* expression in TSAE1 cells treated with vehicle or 4-OHT for 24 h ($n = 4$ biological repeats). **d**, Mean TSAE1 colony size per well ($n = 6$ wells per condition) in Matrigel following treatment with vehicle, 4-OHT or fulvestrant (fulv.) for 7 d in phenol red-free DMEM or medium with charcoal-stripped (CS) fetal bovine serum (FBS). Representative of four independent repeats. AU, arbitrary units. **e**, Primary tumors in BALB/c (TSAE1, EMT6, F3II, D2A1) or FVB (HRM1) mice stained for ER-α (scale bar, 50 µm). **f**, TSAE1 cells injected orthotopically (BALB/c) without ($n = 5$ mice) or with ($n = 6$ mice) estradiol (E2) pellets. **g**, Tumor cells injected orthotopically (TSAE1, EMT6, 4T1, $n = 6$ BALB/c mice per group; HRM1, $n = 5$ FVB mice). Left, tumor growth. Middle, survival analysis. All mice with TSAE1, HRM1 or EMT6 tumors were culled due to primary tumor size limit (solid lines); all mice with 4T1 tumors were culled due to symptoms of metastatic disease (dashed line). Right, hematoxylin and eosin (H&E)-stained lung sections (scale bar, 2.5 mm), with arrowheads indicating small metastatic deposits. **h**, mChLuc2-tagged tumor cells injected orthotopically (TSAE1, $n = 7$ and EMT6, $n = 6$ BALB/c mice; HRM1, $n = 6$ FVB mice). Mice were culled on day 33 (HRM1-mChLuc2 and EMT6-mChLuc2) or day 27 (TSAE1-mChLuc2). Top, representative lung ex vivo IVIS images (scale bar, counts) and H&E-stained lung sections (scale bar, 2.5 mm). Bottom, ex vivo IVIS quantification (total counts). Right, representative images for luciferase-stained TSAE1-mChLuc2 TB lungs (scale bar, 125 µm). **a**,**c**,**f**,**h**, Data are presented as mean values ±s.d. (**a**) or ±s.e.m. (**c**,**f**,**h**); one-way ANOVA with multiple comparisons (**c**), a box plot showing 25th and 75th percentiles, the median (line) and minimum and maximum values (whiskers) (**d**) or two-way ANOVA with multiple comparisons (**f**).

https://doi.org/10.1038/s43018-023-00525-y

of *PDGFC*, *PDGFD* and *PLAT* (encoding tissue plasminogen activator (tPA)), responsible for extracellular cleavage of the PDGF-C precursor[16], was significantly correlated with age and with expression of *EDA2R* and other age-associated genes[15,17], but there was no age-related correlation for *PDGFA* or *PDGFB* (Fig. 2i and Extended Data Fig. 4b).

In the human lung, *PDGFC* is predominantly expressed by fibroblasts and myeloid cells and, to a lesser extent, by epithelial cells[18], findings recapitulated in flow cytometry analysis of the aged mouse lung (Extended Data Fig. 4c). Moreover, expression of *Pdgfc* is elevated in aged primary mouse lung fibroblasts compared to young fibroblasts

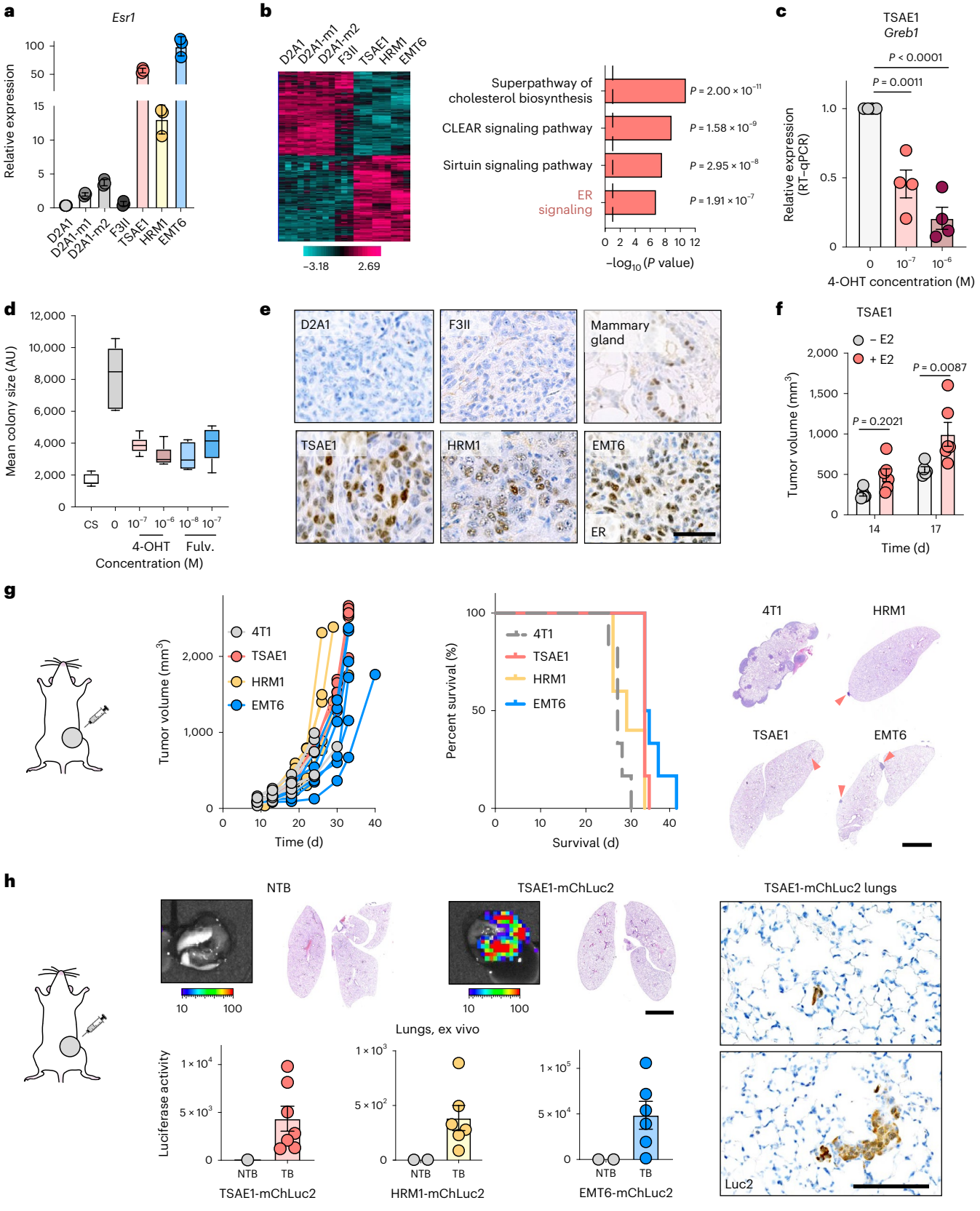

(Fig. 2j). To determine whether the increased level of PDGF-C in fibroblasts from the aged lung promotes metastatic outgrowth of ER$^+$ DTCs, PDGF-C^{hi} CAFs were transduced with non-targeting short hairpin RNA (shRNA) controls (shNTC1 and shNTC2) or shRNA species targeting *Pdgfc* (Extended Data Fig. 4d,e) and inoculated into mice 3 and 8 d after seeding of TSAE1 cells. Mice receiving *Pdgfc*-depleted CAFs displayed reduced metastatic outgrowth (Fig. 2k) and, similarly, control CAFs or fibroblasts from the aged lung but not *Pdgfc*-depleted CAFs or young fibroblasts, supported TSAE1 and HRM1 outgrowth in BME dormancy assays (Extended Data Fig. 4f,g).

Pdgfc expression in the metastatic microenvironment

To assess changes in the metastatic microenvironment, we compared expression of fibrosis-associated genes and PDGF family members in lungs of non-tumor-bearing (NTB) young and aged mice (from Fig. 2d) with parallel cohorts of young and aged mice inoculated orthotopically with TSAE1 tumor cells (tumor-bearing (TB) mice). Consistent with the presence of limited metastatic disease in young TB mice and macrometastatic lesions in aged TB lungs (Fig. 2a and Extended Data Fig. 5a), aged TB lungs had a higher TSAE1 tumor signature score, a pattern paralleled by increased expression of fibroblast activation and fibrosis genes, indicating further activation of the microenvironment in the presence of metastatic disease (Fig. 3a). Notably, expression of *Pdgfc* and *Plat* is further elevated in TB lungs of aged mice, whereas levels of other PDGF family members are further reduced (Fig. 3b).

In ER$^-$ breast cancer, tumor cell-derived PDGF-C has been demonstrated to promote CAF recruitment[19,20]. However, the role of PDGF-C in ER$^+$ breast cancer has been largely overlooked, mainly due to low expression of *PDGFC* in ER$^+$ human breast cancer cell lines in vitro[20]. Indeed, expression of *PDGFC* was inversely correlated with *ESR1* expression in breast cancer cell lines (Fig. 3c), and *Pdgfc* expression was significantly lower in cultured ER$^+$ TSAE1 and HRM1 tumor cells than in ER$^-$ D2A1 and 4T1 cells (Fig. 3d). The situation is less clear in human tumors, with the Molecular Taxonomy of Breast Cancer International Consortium (METABRIC) dataset revealing higher *PDGFC* expression in ER$^+$ breast cancers than in ER$^-$ breast cancers (Fig. 3e). As METABRIC is a bulk tumor analysis, it is not possible to differentiate between tumor cell and stromal *PDGFC* expression; however, single-cell RNA-seq analysis of 26 human breast cancers[21] demonstrated comparable *PDGFC* expression across ER$^+$ and ER$^-$ tumor cells, with ER$^+$ cells expressing markedly higher levels of *PLAT* (Extended Data Fig. 5b). Furthermore, *Pdgfc* in situ hybridization (RNAscope) of TSAE1 TB young and aged mice revealed extensive upregulation of *Pdgfc* in primary tumors and metastatic lesions in the aged lungs (Fig. 3f), together raising the possibility that tumor cells contribute to increased *Pdgfc* expression in aged TB mouse lungs.

To address this, TSAE1-mChLuc2 tumor cells were sorted from primary tumors and from lungs with metastatic lesions. Compared to cells in culture, *Pdgfc* expression was significantly elevated in ER$^+$ tumor cells in vivo, whereas *Pdgfa* and *Pdgfb* were not (Fig. 3g and Extended Data Fig. 6a). Similarly, tumor cell *PDGFC*, assessed using a human-specific *PDGFC* probe, was upregulated in ER$^+$ ZR-75-1 tumors compared to ZR-75-1 cells in culture (Extended Data Fig. 6b). By contrast, PDGF-C^{hi}ER$^-$ D2A1 and 4T1 cells did not display further upregulation of *Pdgfc* expression in vivo (Fig. 3h). Strikingly, TSAE1 cells isolated from young and aged lungs demonstrated significantly elevated tumor cell number and tumor cell *Pdgfc* expression in aged compared to young TB lungs (Fig. 3i), indicating that *Pdgfc* expression is upregulated in ER$^+$ tumor cells in metastatic lesions compared to dormant DTCs. At least in part, this likely reflects the activated microenvironment associated with macrometastatic lesions as *Pdgfc* or *PDGFC* expression by ER$^+$ tumor cells could be induced by co-culture with PDGF-C^{hi} CAFs (Extended Data Fig. 6c). Conversely, PDGF-C^{hi}ER$^-$ 4T1 and AT-3 cells did not display increased metastatic colonization in aged BALB/c and C57BL/6 mice, respectively, indicating that their high endogenous *Pdgfc* expression was sufficient to initiate metastatic colonization in the PDGF-C^{lo} microenvironment of young lungs (Extended Data Fig. 6d–f).

Tumor cell PDGF-C supports DTC survival and outgrowth

To test whether tumor cell-derived PDGF-C in growing metastatic lesions contributes to the development of a productive metastatic niche, TSAE1 cells were transduced with shNTC1 or shNTC2 or with two independent shRNA species targeting *Pdgfc* (shPdgfc1, shPdgfc5). All shRNA lines displayed comparable growth rate in vitro (Fig. 4a,b). As previously shown, the higher number of ER$^+$ TSAE1 cells disseminating to the lung following intravenous inoculation partly overcame the deficiency of a PDGF-C^{lo} microenvironment (Fig. 2c,e), and, in these assays, *Pdgfc* knockdown significantly limited metastatic outgrowth (Fig. 4c), a finding recapitulated in the HRM1 ER$^+$ model (Fig. 4d and Extended Data Fig. 7a,b). Importantly, in the bleomycin-induced lung fibrosis model, in which stromal PDGF-C levels are elevated and the lung microenvironment is extensively activated (Fig. 2h and Extended Data Fig. 3e–g), TSAE1-shPdgfc and TSAE1-shNTC cells displayed comparable metastatic outgrowth (Fig. 4e). When inoculated orthotopically, TSAE1-shNTC and TSAE1-shPdgfc primary tumors grew comparably in young mice (Fig. 4f), with immunohistochemical analysis confirming that *Pdgfc* knockdown was maintained in vivo (Extended Data Fig. 7c). As previously observed (Figs. 1g,h and 2b), young mice with TSAE1-shNTC tumors displayed evidence of dormant disseminated disease with few macrometastatic lesions. Depletion of *Pdgfc* further reduced this metastatic colonization (Fig. 4f), indicating a role for low-level tumor-derived PDGF-C in ER$^+$ DTC survival. Finally, in support of the need for a PDGF-C^{hi} microenvironment for dormant DTC outgrowth, overexpression of *Pdgfc* (Fig. 4g), which had no impact on cell proliferation in vitro or primary tumor growth, significantly increased metastatic burden (Fig. 4h).

Fig. 2 | An aged microenvironment supports ER$^+$ DTC metastatic outgrowth. All experiments used TSAE1 cells inoculated into BALB/c mice. **a**, Orthotopic inoculation into young or aged (15-month-old) mice ($n = 6$ mice per group). Left, tumor growth. Right, quantification of lung metastatic burden (day 30) and representative images (scale bar, 1 mm). Additional quantification is shown in Extended Data Fig. 3a. **b**, Orthotopic inoculation into $n = 4$ young or $n = 3$ aged (>12-month-old) mice. EdU was injected 24 h before culling (day 33), and EdU$^+$ tumor cells in formalin-fixed paraffin-embedded (FFPE) tissue sections were quantified; representative images are shown (scale bar, 100 µm). Additional images are shown in Extended Data Fig. 3b. **c**, Intravenous inoculation into $n = 5$ young and $n = 4$ aged (9-month-old) mice. Metastatic lung burden (day 15), images (scale bar, 2.5 mm). **d**, RNA-seq profiling of NTB lungs from young (12-week-old) and aged (13-month-old) mice ($n = 5$ mice per group). Left, hierarchical clustering. Right, expression of 'fibroblast-activation signature' and 'fibrosis signature' genes. **e**, Intravenous inoculation into young mice 3 d after vehicle or bleomycin treatment ($n = 6$ mice per group). Metastatic lung burden (15 d after inoculation), representative images (scale, 2.5 mm). **f**, Orthotopic inoculation into young mice (day 1), treated with vehicle or bleomycin starting at day 10 ($n = 6$ mice per group). Metastatic lung burden (day 32), representative images (scale, 2.5 mm). **g**, Expression in NTB lungs of young and aged mice (RNA-seq). **h**, NTB mice treated with vehicle or bleomycin and culled 7 or 14 d later ($n = 3$ mice per group; RT–qPCR). **i**, Correlation analysis of *PDGFC* and *EDA2R* expression in human non-cancerous lung samples ($n = 1{,}197$ patients; GSE23546). DEG, differentially expressed gene; FDR, false discovery rate. **j**, *Pdgfc* expression (RT–qPCR) in primary fibroblasts (three independent repeats). **k**, Intravenous inoculation into young mice. On days 3 and 8, mice were injected intravenously with shNTC- or shPdgfc mouse GFP$^+$ CAFs ($n = 5$ mice per group). Metastatic lung burden (day 10; shNTC and shPdgfc, $n = 10$ mice per group). **a**–**c**,**e**,**f**,**h**,**j**,**k**, Data are presented as mean values ± s.e.m.; two-tailed Mann–Whitney *U*-test (**a**,**k**), two-tailed *t*-test (**b**,**c**,**e**,**f**,**j**), two-tailed Pearson's correlation (**i**) or two-way ANOVA with multiple comparisons (**h**).

https://doi.org/10.1038/s43018-023-00525-y

PDGF-C-mediated fibroblast activation

Expression of the PDGF-C receptor encoded by *PDGFRA* is restricted to fibroblasts in normal lung tissue (the Human Protein Atlas, http://www.proteinatlas.org[18]) and primary human breast cancers[21] (Extended Data Fig. 8a). Similarly, in the ER$^+$ tumor cells used here, *Pdgfra* and *PDGFRA* mRNA and PDGFRα protein levels are negligible compared to those in mouse (CAF, 10T1/2) or human (MRC5) fibroblasts (Fig. 5a,b). Indeed, recombinant PDGF-C (rPDGF-C) treatment of fibroblasts but not ER$^+$ tumor cells promoted PDGFRα, AKT, ERK and S6 phosphorylation, which was suppressed by the PDGFRα inhibitor imatinib (Fig. 5b), and, consistent with previous reports[22–24], fibroblast proliferation and migration increased following rPDGF-C treatment (Fig. 5c and Extended Data Fig. 8b,c). RNA-seq profiling of rPDGF-C-treated MRC5 fibroblasts and analysis of the secreted transcriptome identified enrichment of fibrotic and wound-healing pathways as well as increased *PLAT* expression (Fig. 5d and Extended Data Fig. 8d). PDGF-C has been reported to drive accumulation of perivascular CAFs[25], but we observed no difference in vessel density or pericyte or perivascular CAF coverage in TSAE1 primary tumors from cells transduced with shNTC or shPdgfc (Extended Data Fig. 9a) nor the number of activated

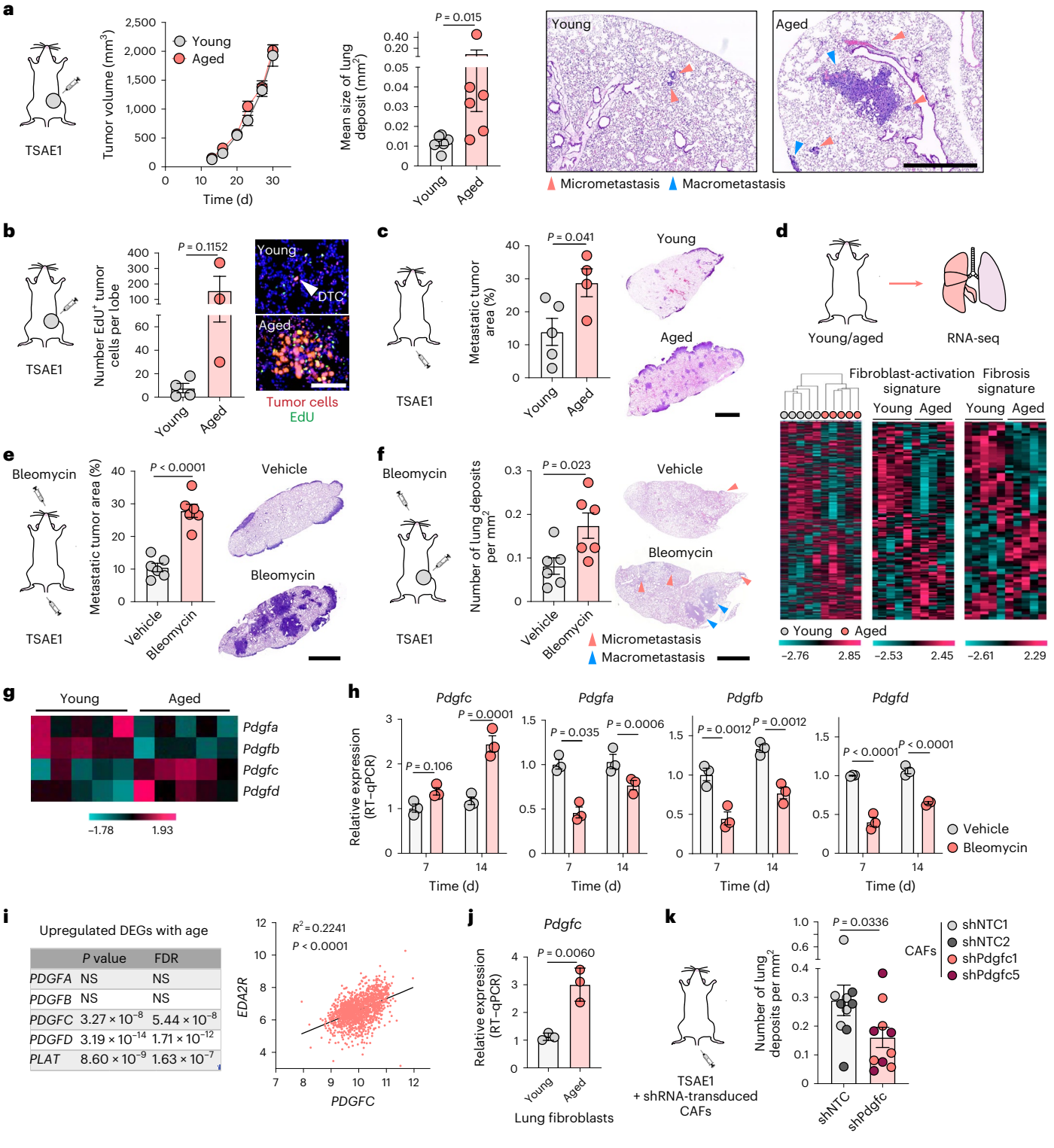

	P value	FDR
PDGFA	NS	NS
PDGFB	NS	NS
PDGFC	3.27×10^{-8}	5.44×10^{-8}
PDGFD	3.19×10^{-14}	1.71×10^{-12}
PLAT	8.60×10^{-9}	1.63×10^{-7}

https://doi.org/10.1038/s43018-023-00525-y

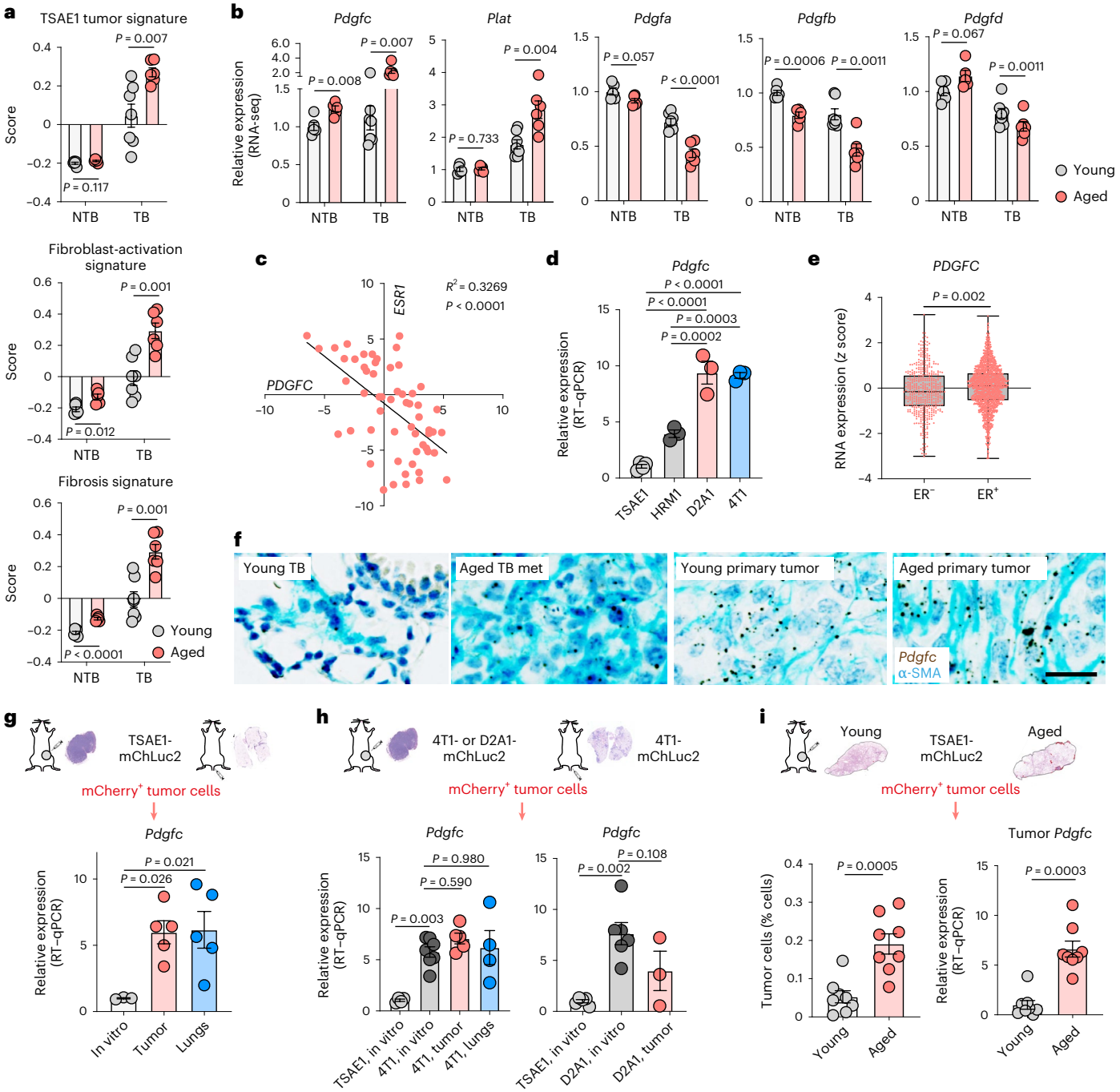

Fig. 3 | ER⁺ tumor cells contribute to elevated PDGF-C in the metastatic microenvironment. a,**b**, RNA-seq profiling of lungs from young or aged (13-month-old) BALB/c mice ($n = 7$ or $n = 6$ mice, respectively) inoculated orthotopically with TSAE1 cells (TB; day 29). NTB mice are from Fig. 2d. See Extended Data Fig. 5a for histology. **a**, Scores for TSAE1 tumor signature, fibroblast-activation signature and fibrosis signature (Methods). **b**, *Pdgfa*–*Pdgfd* and *Plat* expression. **c**, Correlation analysis of *ESR1* and *PDGFC* expression in human breast cancer cell lines (Cancer Cell Line Encyclopedia (CCLE)). **d**, *Pdgfc* expression (RT–qPCR) in mouse tumor lines in vitro (three independent repeats; TSAE1, four). **e**, *PDGFC* expression in human breast cancers (METABRIC dataset; ER⁻, $n = 445$ patients; ER⁺, $n = 1{,}459$ patients). **f**, *Pdgfc* RNAscope analysis of mouse tissue from **a**,**b**; counterstained for α-SMA (cyan). Representative images of TB young mouse lungs, metastatic deposits (met) in TB aged lungs and primary tumors (scale bar, 25 µm). **g**–**i**, mChLuc2-tagged tumor cells were isolated by flow cytometry from primary (orthotopic inoculation) and metastatic (intravenous inoculation) tumors in young mice. **g**, *Pdgfc* expression in TSAE1-mChLuc2 cells (day 16, orthotopic; day 15, intravenous; $n = 5$ mice per group) compared to cells in vitro ($n = 3$ biological repeats). **h**, Left, *Pdgfc* expression in 4T1-mChLuc2 cells from primary tumors (day 14, $n = 5$ mice), or lung metastases (day 10, $n = 4$ mice), compared to in vitro cultures (TSAE1, $n = 4$; 4T1, $n = 7$ biological repeats). Right, *Pdgfc* expression in D2A1-mChLuc2 cells from primary tumors (days 20–25, $n = 3$ mice) compared to in vitro cultures (TSAE1, $n = 5$; D2A1, $n = 6$ biological repeats). **i**, TSAE1-mChLuc2 cells inoculated orthotopically into young or aged (10–13-month-old) mice. mCherry⁺ tumor cells were isolated from the lungs (days 31–35; $n = 8$ mice per group). Left, tumor cell quantification. Right, *Pdgfc* expression in isolated tumor cells. **a**,**b**,**d**,**g**–**i**, Data are presented as mean values ± s.e.m.; multiple *t*-tests (**a**,**b**), Pearson's correlation (two tailed) (**c**), one-way ANOVA with multiple comparisons (**d**,**g**,**h**), a box plot showing 25th and 75th percentiles, the median (line) and minimum and maximum values (whiskers) (**e**), two-tailed *t*-test (**e**,**i**, left) or two-tailed Mann–Whitney *U*-test (**i**, right).

(α smooth muscle actin (α-SMA)$^+$) fibroblasts (Extended Data Fig. 9b). However, there were significantly fewer α-SMA$^+$ fibroblasts in shPdgfc metastatic lesions following intravenous inoculation of TSAE1 or HRM1 cells (Fig. 5e,f and Extended Data Fig. 9c), indicating that, in the young lung microenvironment, tumor-derived PDGF-C is required to promote fibroblast recruitment and activation.

Role of PDGF-C in a human ER$^+$ model of metastatic relapse

To extend these studies to human breast cancer, we employed the human ER$^+$ breast cancer cell line ZR-75-1. Despite being inoculated orthotopically into NOD SCID gamma (NSG) mice lacking a functional immune system, ZR-75-1 cells were found only as single DTCs or small cell clusters in the lungs with little evidence of dissemination to other organs (Fig. 6a and Extended Data Fig. 10a). Following lung dissociation, isolated ZR-75-1 cells remained non-proliferative in vitro but could be reactivated with fibroblast CM (Fig. 6a), findings consistent with in vitro dormancy assays (Extended Data Fig. 2b–d). When injected intravenously, ZR-75-1 cells disseminated to the lungs and remained largely dormant; however, tumor cells disseminating to the liver and bone, other common sites of metastasis in breast cancer, eventually formed macrometastases (Fig. 6b and Extended Data Fig. 10b). *PDGFC* RNAscope, using a human-specific probe (Extended Data Fig. 10c), confirmed quantitative PCR with reverse transcription (RT–qPCR) analysis of isolated tumor cells (Extended Data Fig. 6b), showing upregulated *PDGFC* expression in ZR-75-1 primary tumor cells but low-level *PDGFC* expression by DTCs, again supporting the contention that dormant DTCs are PDGF-C^{lo}. Generation of two independent ZR-75-1-shPDGFC lines confirmed that downregulation of *PDGFC* does not impact tumor cell proliferation in vitro (Extended Data Fig. 10d) but, following intravenous inoculation, significantly reduces the number of single DTCs and larger lesions (Fig. 6c and Extended Data Fig. 10e). Conversely, pre-conditioning lungs of young mice with rPDGF-C or bleomycin promoted DTC proliferation (Fig. 6d). Together, these findings demonstrate a critical role for tumor cell-derived PDGF-C in supporting both DTC (PDGF-C^{lo}) survival and metastatic (PDGF-C^{hi}) outgrowth. This role of PDGF-C is further evidenced in the spontaneous metastasis setting with ZR-75-1 cells ectopically expressing *Pdgfc* disseminating to the lungs and, instead of only remaining as single dormant cells (Fig. 6a), forming metastatic deposits (Fig. 6e and Extended Data Fig. 10f).

PDGF-C signaling blockade impairs ER$^+$ metastatic outgrowth

Given the role of tumor-derived *Pdgfc* in ER$^+$ DTC survival and outgrowth, we assessed whether pharmacological inhibition of PDGFRα using imatinib limits metastatic outgrowth. As expected, given the fibroblast-restricted *Pdgfra* and *PDGFRA* expression, imatinib impacted on CAF but not tumor cell viability (Fig. 7a). Imatinib treatment of mice inoculated intravenously with TSAE1 cells suppressed metastatic outgrowth in the lungs and reduced fibroblast activation in metastatic lesions (Fig. 7b and Extended Data Fig. 10g). Similarly, imatinib treatment significantly lowered ZR-75-1 whole-body metastasis with a trend for less metastatic outgrowth in the livers and a smaller proportion of DTCs in the lungs developing into tumor cell clusters (Fig. 7c). As previously shown (Fig. 4c), *Pdgfc* depletion in TSAE1 cells severely impaired metastatic outgrowth (Fig. 7d), and, when combined with imatinib treatment, there was a small but non-significant additional reduction in lung tumor cell content, likely due, at least in part, to imatinib inhibiting PDGFRα on fibroblasts that will respond both to tumor cell- and non-tumor cell-derived PDGF-C. Finally, we sought to determine whether targeting PDGF-C signaling in PDGF-C^{hi} fibrotic and aged lungs could suppress metastatic outgrowth of ER$^+$ DTCs. Treating fibrotic lungs with imatinib before TSAE1 cell inoculation or with a PDGF-C-blocking antibody, shown to block PDGF-C signaling in vivo[25,26], from the day of TSAE1 inoculation was equally effective at reducing metastatic outgrowth (Fig. 8a,b). Similarly, the PDGF-C-blocking antibody significantly reduced the increased metastatic outgrowth observed in aged mice (Fig. 8c).

In summary (Fig. 8d), these data demonstrate that low-level *Pdgfc* expression in ER$^+$ DTCs aids their survival but is insufficient for generation of a metastasis-permissive niche in healthy young lungs. Conversely, in aged or fibrotic lungs, the activated PDGF-C^{hi} stroma supports metastatic outgrowth, highlighting inhibition of PDGF-C signaling as an opportunity to limit metastatic relapse in ER$^+$ breast cancers.

Discussion

Risk of late recurrence in patients with ER$^+$ breast cancer is dependent on initial clinicopathological diagnosis; however, even those with low-grade node-negative (T1N0) tumors have a 10–17% risk of distant recurrence in the following 5–20 years[2]. Despite this continuing risk, our understanding of late ER$^+$ metastatic relapse remains limited by the lack of suitable preclinical models. Here, we use ER$^+$ mouse mammary tumor cell lines and demonstrate that, in syngeneic young immunocompetent mice, without additional estrogen supplementation to better model the hormonal environment in older women, cells from the primary tumor disseminate to secondary sites but inefficiently develop into macrometastatic lesions. By contrast, to mimic age-associated microenvironmental changes, parallel experiments in aged mice or mice with fibrotic lungs reveal accelerated metastatic outgrowth.

Using these models, we sought to identify factors upregulated in pro-metastatic aged mouse lungs. RNA-seq analysis reveals a plethora of genes associated with fibroblast activation and development of fibrosis, previously reported to promote metastatic colonization[27]. However, of particular interest are the discordant patterns of expression of the four members of the PDGF family of growth factors. The function of PDGFs in cancers of epithelial origin has been described primarily with regard to activation of fibroblasts and/or promotion of angiogenesis[28,29]. However, few studies have examined the role of PDGFs in metastasis. Intriguingly, our studies demonstrate that, while expression of the classical PDGFs *Pdgfa* and *Pdgfb* is downregulated in aging (both NTB and TB) and fibrotic lungs, expression of *Pdgfc* and *Plat* (tPA), encoding the proteolytic enzyme required for PDGF-C activation, is strongly upregulated.

In the normal lung, liver and bone, the main sites of ER$^+$ breast cancer recurrence, levels of PDGF-C are low (the Human Protein Atlas[18,30]). By comparison, in diseased tissue, increased PDGF-C levels have been reported in subsets of macrophages[25,26], CAFs[31,32] and tumor cells[19,33,34]. Here, we demonstrate that *PDGFC* and *Pdgfc* expression by ER$^+$ cells is elevated in primary tumors and established metastatic lesions but remains low in non-proliferative DTCs at secondary sites. However, this low-level *Pdgfc* expression plays an important functional role as tumor cell *Pdgfc* depletion significantly diminishes ER$^+$ DTC survival. Conversely, ectopic expression of *Pdgfc* in ER$^+$ cells enhances metastatic outgrowth, indicating that the level of ER$^+$ DTC-derived PDGF-C alone is insufficient for effective metastatic outgrowth. This deficiency is overcome in the PDGF-C^{hi} lung microenvironment of aged or fibrotic mice or by pre-conditioning lungs of young mice by intranasal administration of rPDGF-C. Importantly, this deficiency is not evident with PDGF-C^{hi}ER$^-$ 4T1 and AT-3 lines, which display equivalent metastatic outgrowth in both young and aged mice. In triple-negative breast cancers, age at diagnosis is associated with adverse prognosis with patients <40 years old having worse outcome[35]. Although other factors such as delayed detection undoubtedly contribute to poor prognosis, the prognostic effect remained significant in multivariant analysis[35] and is further supported by mouse models, with triple-negative breast xenografts displaying earlier onset and enhanced growth in young (8–10-week-old) mice compared to their aged (>10-month-old) counterparts[36] and the equivalent metastatic outgrowth of ER$^-$ cell lines in young and aged mice as reported here.

In support of our data in the ER$^+$ setting, there is a growing body of evidence describing a role for the aged stroma, including the immune cells, fibroblasts and extracellular matrix, in promoting tumorigenesis[37]. The immune compartment can regulate the balance

https://doi.org/10.1038/s43018-023-00525-y

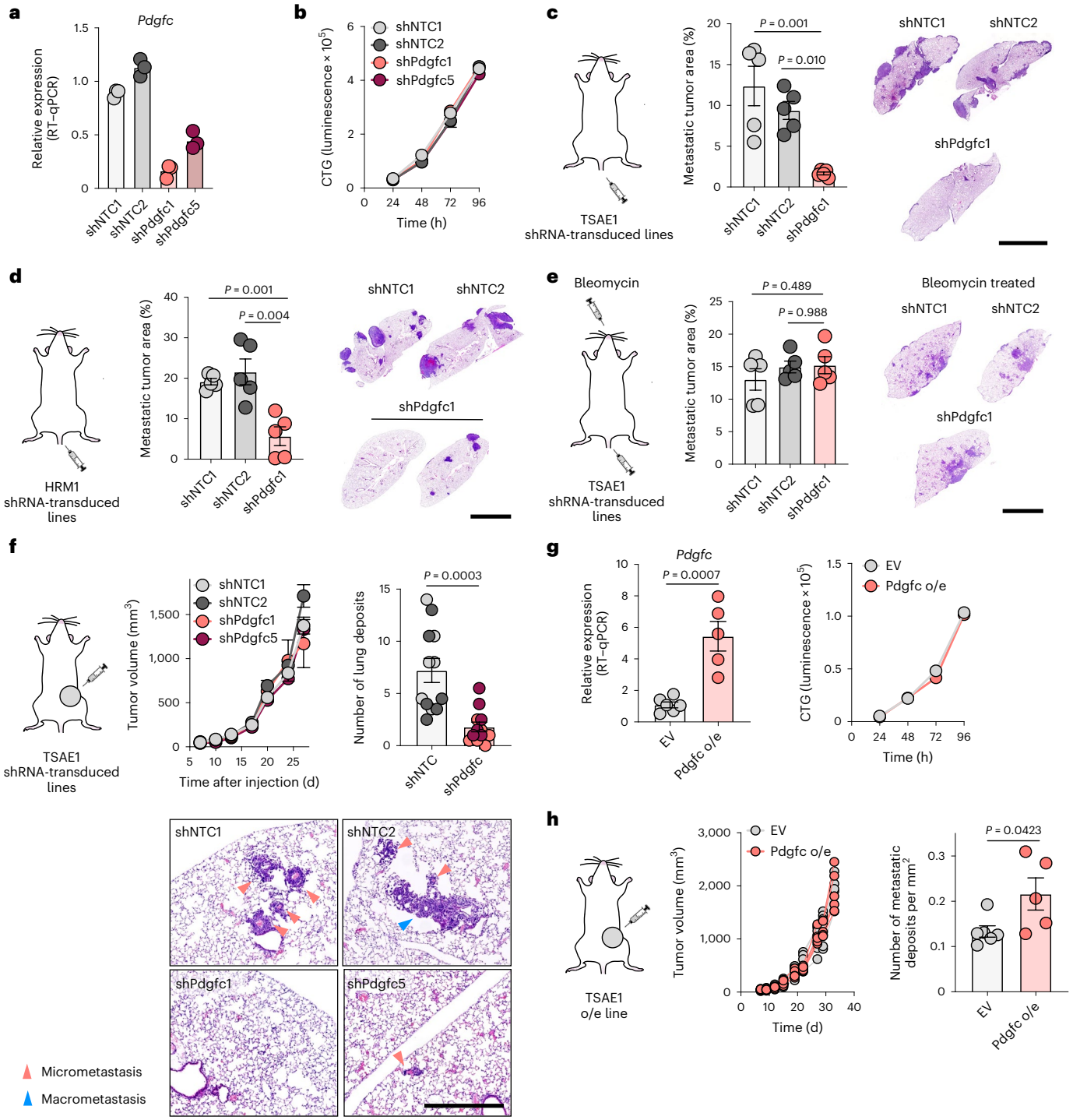

Fig. 4 | Tumor cell-derived PDGF-C in ER$^+$ metastatic outgrowth. a, *Pdgfc* expression (RT–qPCR) in TSAE1 cells transduced with shNTC1, shNTC2, shPdgfc1 or shPdgfc5. Representative of five independent repeats. **b**, In vitro proliferation of TSAE1 cells transduced with shNTC or shPdgfc. Representative of two independent repeats. **c**, TSAE1 cells transduced with shNTC or shPdgfc were injected intravenously into young BALB/c mice ($n = 5$ mice per group). Metastatic lung burden (day 14), with representative H&E-stained sections (scale bar, 5 mm). **d**, HRM1 cells transduced with shNTC or shPdgfc (Extended Data Fig. 7a,b) were injected intravenously into young FVB mice ($n = 5$ mice per group). Metastatic lung burden (day 30). Two mice with shPdgfc tumors had no metastatic deposits. Representative H&E-stained sections (scale bar, 5 mm). **e**, TSAE1 cells transduced with shNTC or shPdgfc were injected intravenously into bleomycin-treated young BALB/c mice ($n = 5$ mice per group) as described in Fig. 2e. Metastatic lung burden (day 11 after TSAE1 inoculation), with representative H&E-stained sections (scale bar, 5 mm). **f**, TSAE1 cells transduced with shNTC or shPdgfc were injected orthotopically into young BALB/c mice ($n = 6$ mice per group). Left, tumor growth. Right, quantification of lung metastatic deposits (day 28; shNTC and shPdgfc, $n = 12$ mice per group). Bottom, representative H&E-stained sections (scale bar, 500 µm). See Extended Data Fig. 9a,b for primary tumor immunostaining. **g**, TSAE1 cells carrying control vector (EV) or expressing *Pdgfc* (Pdgfc o/e). Left, *Pdgfc* expression (RT–qPCR) in TSAE1 tumors (EV, $n = 6$ mice; *Pdgfc* overexpression, $n = 5$ mice). Right, in vitro proliferation. Representative of two independent repeats. **h**, Young BALB/c mice were injected orthotopically with TSAE1 cells carrying EV ($n = 6$ mice) or overexpressing (o/e) *Pdgfc* ($n = 5$ mice). Mice were culled on days 30–35. Left, tumor growth for individual mice. Right, quantification of lung metastatic deposits. Data are presented as mean values ± s.e.m. (**c**–**h**); one-way ANOVA with multiple comparisons (**c**–**e**) or two-tailed *t*-test (**f**–**h**).

https://doi.org/10.1038/s43018-023-00525-y

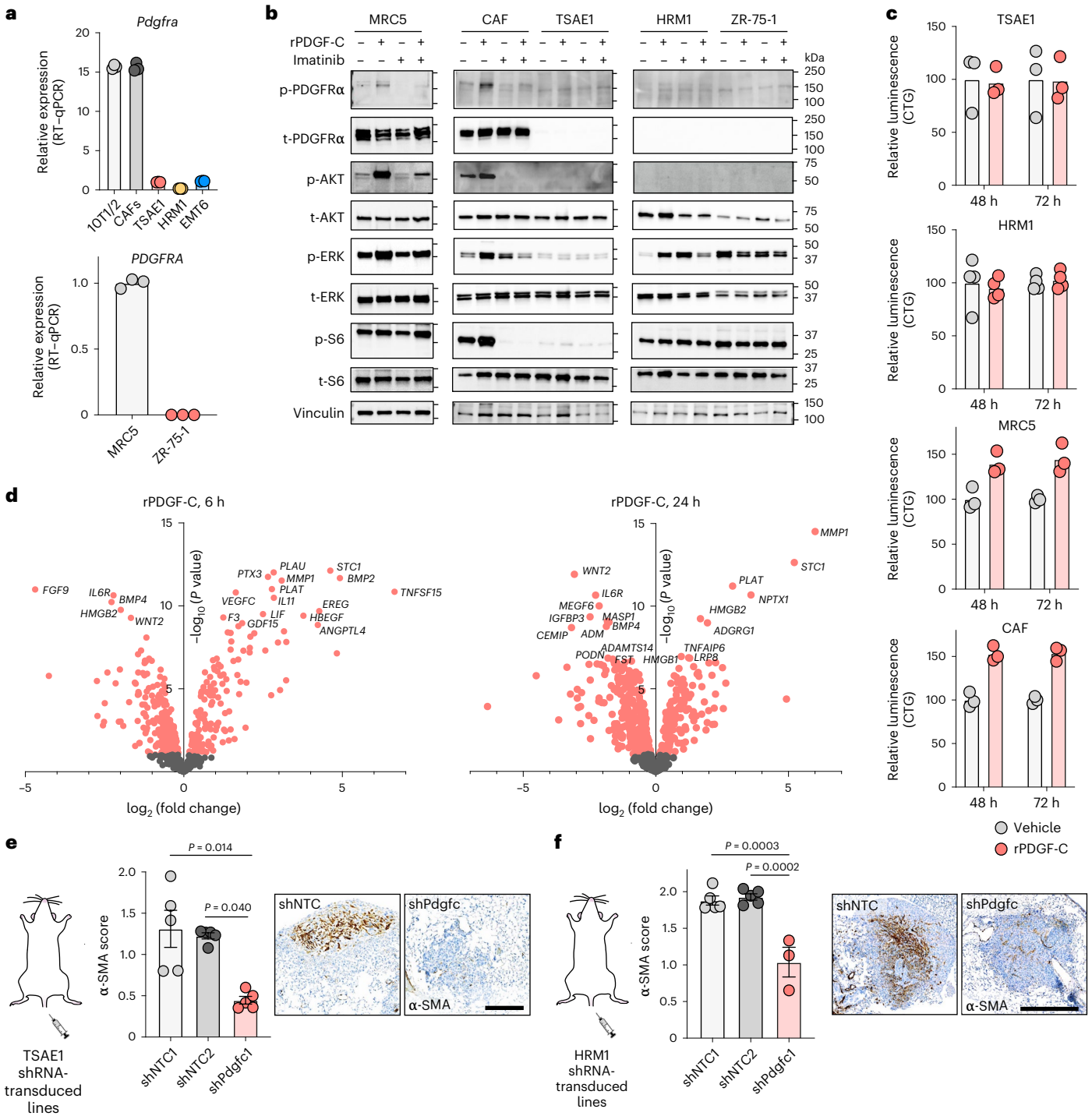

Fig. 5 | PDGF-C signals through PDGFRα to activate fibroblasts. a, *Pdgfra* and *PDGFRA* expression (RT–qPCR) in mouse (top) and human (bottom) fibroblasts (gray) and tumor cell lines (colored). Representative data of two independent repeats, multiple cell lines. **b**, Western blot analysis of fibroblasts and ER$^+$ tumor cells following treatment with vehicle, rPDGF-C (100 ng ml^{-1}) and/or imatinib (1 µM). Representative data of two independent repeats, multiple cell lines. p, phosphorylated; t, total. **c**, CellTiter-Glo (CTG) analysis of fibroblasts and ER$^+$ tumor cells treated with vehicle or rPDGF-C (100 ng ml^{-1}). Representative data from two (HRM1), three (TSAE1, CAF) and six (MRC5) independent repeats per cell line. **d**, RNA-seq analysis of MRC5 fibroblasts treated with vehicle or rPDGF-C for 6 h (left) or 24 h (right). Genes differentially expressed following treatment (two-tailed *t*-test, $P < 0.01$) are highlighted in red with the top 20 significantly altered genes labeled. **e**,**f**, Lungs from BALB/c mice were injected intravenously with TSAE1 tumor cells (from Fig. 4c), or FVB mice were injected intravenously with HRM1 tumor cells (from Fig. 4d), respectively, and stained for α-SMA. Metastatic deposits were scored for the number of α-SMA$^+$ cells (Extended Data Fig. 9c). Representative images (scale bar, 500 µm). Note that two HRM1-shPdgfc mice had no detectable lung deposits (Fig. 4d). Data are presented as mean values; ±s.e.m., Kruskal–Wallis test with multiple comparisons (**e**,**f**).

between DTC dormancy and metastatic outgrowth[5,6,38] and, when altered in human and mouse aging, has implications for therapy response and metastatic control[37]. In parallel, aging fibroblasts display an altered secretome, with secretion of the Wnt antagonists secreted frizzled-related protein (sFRP)1 and sFRP2 promoting metastatic outgrowth[17,39], and, similarly, intranasal administration of transforming

https://doi.org/10.1038/s43018-023-00525-y

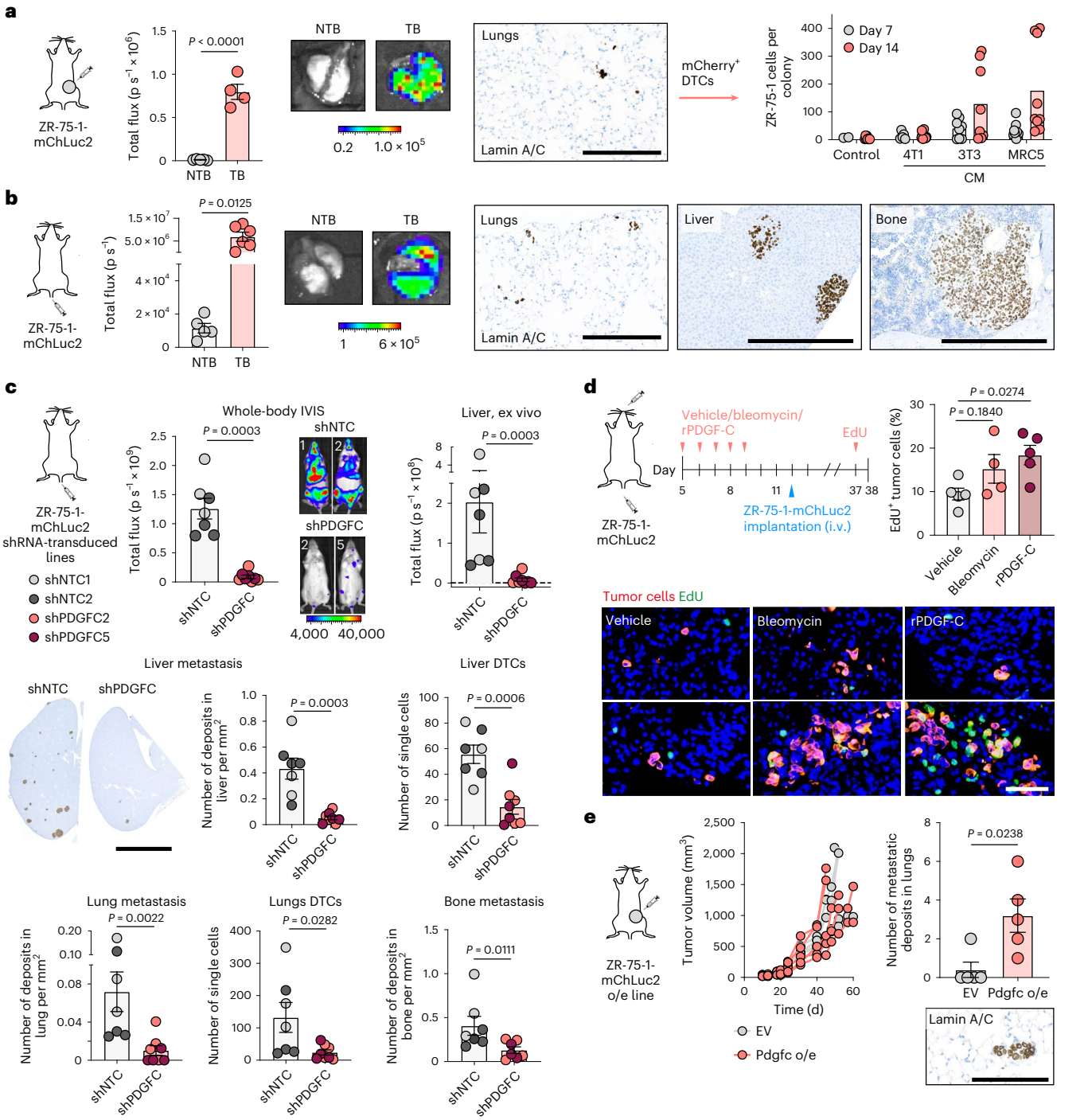

Fig. 6 | Tumor-derived PDGF-C is required for metastatic outgrowth. All experiments involved ZR-75-1-mChLuc2 cells inoculated into young NSG mice. **a**, Orthotopic inoculation (TB), with NTB controls ($n = 5$ mice per group). Left, ex vivo IVIS imaging of lungs (days 34–43; $n = 4$ TB mice as one mouse was used for tumor cell isolation; scale bar, radiance, p s^{-1} cm^{-2} sr^{-1}). Right, TB lungs stained for human lamin A/C (scale bar, 250 µm). Tumor cells sorted from lungs ($n = 1$ TB mouse) were treated with control medium or 4T1 or fibroblast (MRC5 or 3T3) CM. Number of cells per colony (days 7 and 14). **b**, Intravenous inoculation (TB; $n = 6$ mice). Left, ex vivo IVIS imaging of lungs (day 29; scale bar, radiance, p s^{-1} cm^{-2} sr^{-1}). NTB control mice were from **a**. Right, human lamin A/C staining of lungs, liver and hind leg bones (scale bars; lungs, 250 µm; liver and bones, 500 µm). **c**, Cells transduced with shNTC1, shNTC2, shPDGFC2 or shPDGFC5 were injected intravenously (shNTCs and shPDGFCs; $n = 7$ or 8 mice per group, respectively). Top left, whole-body IVIS signal (day 28; scale bar, counts). Top right, ex vivo IVIS signal in livers (day 29). Bottom left, quantification of metastatic deposits and DTCs with representative human lamin A/C-stained liver sections (scale bar, 5 mm). Only three shPDGFC5 hind leg bone samples were available. **d**, Mice were treated daily for 5 d with vehicle, bleomycin or rPDGF-C. On day 12, ZR-75-1-mChLuc2 cells were inoculated intravenously (i.v.) ($n = 5$ vehicle- or rPDGF-C-treated mice; $n = 4$ bleomycin-treated mice). Mice were injected with EdU (day 37) and culled 24 h later. Percentage of EdU^+ human ($lamin\ A/C^+$) tumor cells, representative images (scale bar, 50 µm). **e**, Cells carrying EV or overexpressing (o/e) *Pdgfc* cells were injected orthotopically ($n = 5$ mice per group). Mice were culled on days 45–60. Left, tumor growth for individual mice. Right, quantification of lung metastatic deposits, with representative human lamin A/C staining (scale bar, 125 µm). Data are presented as mean values; ±s.e.m. (**a**, left; **b**–**e**, right); two-tailed *t*-test (**a**–**c**, middle right), one-way ANOVA with multiple comparisons (**d**) or two-tailed Mann–Whitney *U*-test (**c**, top, middle left, bottom; **e**).

https://doi.org/10.1038/s43018-023-00525-y

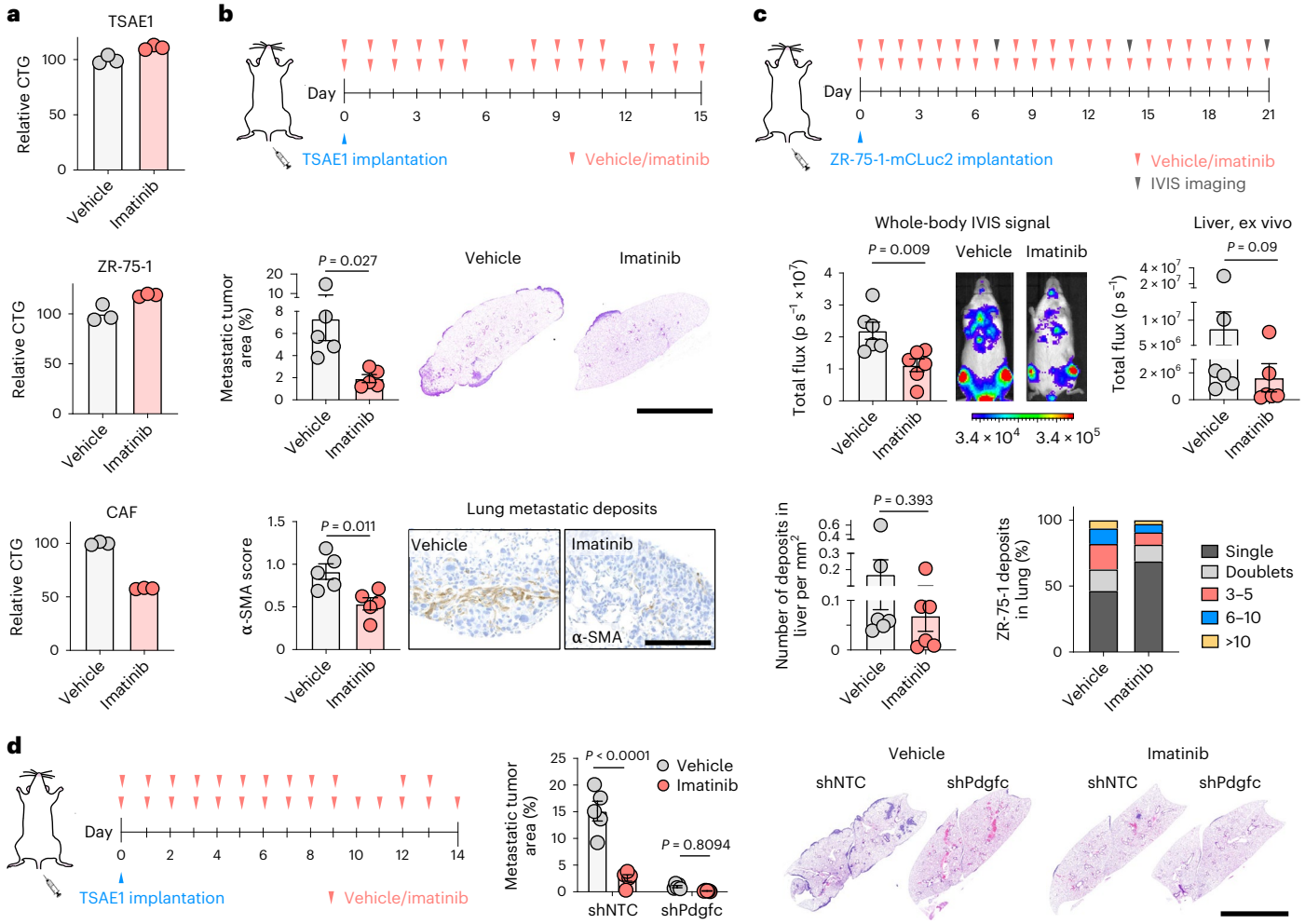

Fig. 7 | Pharmacological inhibition of PDGFRα with imatinib limits metastatic outgrowth of ER$^+$ DTCs. a, CellTiter-Glo analysis of ER$^+$ tumor cells and fibroblasts after 72 h of vehicle or imatinib (1 μM) treatment (representative data of two independent repeats, multiple cell lines). **b**, TSAE1 cells were injected intravenously into young BALB/c mice, with mice receiving vehicle or imatinib as indicated ($n = 5$ mice per group). Middle, lung metastatic burden (day 15), with representative lung sections (scale bar, 5 mm). Bottom, lungs were stained for α-SMA, and metastatic deposits were scored for the number of α-SMA-positive cells (Extended Data Fig. 10g), with representative images (scale bar, 500 μm). **c**, ZR-75-1-mChLuc2 cells were injected intravenously into young NSG mice, with mice receiving vehicle or imatinib treatment as indicated ($n = 6$ mice per group). Middle left, whole-body IVIS signal on day 14. IVIS signal quantification, with representative images (scale bar shows radiance, p s^{-1} cm^{-2} sr^{-1}). Middle right, quantification of ex vivo IVIS signal in livers (day 21). Bottom left, number of liver metastatic deposits. Bottom right, percentage of tumor deposits in the lungs that are single cells, doublets, 3–5 tumor cells, 6–10 tumor cells or >10 tumor cells. **d**, TSAE1 tumor cells transduced with shNTC1 or shPdgfc1 were inoculated intravenously into young BALB/c mice, which were treated with vehicle or imatinib as indicated ($n = 5$ mice per group). Metastatic lung burden (day 14), with representative lung sections shown (scale bar, 5 mm). Data are presented as mean values; ±s.e.m. (**b**–**d**); two-tailed *t*-test (**b**,**c** (top left)), two-tailed Mann–Whitney *U*-test (**c**, top right and bottom) or two-way ANOVA with multiple comparisons (**d**).

growth factor (TGF)-β creates a fibrotic environment, supporting outgrowth of breast tumor cells in the lungs[4]. Here, we describe upregulated expression of *Pdgfc* in aged mouse fibroblasts and a strong correlation between *PDGFC* expression and expression of age-related genes in a large dataset of human lung samples. It is important to note that the 12–16-month-old mice used here and in other studies of the aging microenvironment[17,39] are considered equivalent to middle-aged or late middle-aged women (https://www.jax.org). As expression of age-related genes continues to increase with age in human populations[15], it is anticipated that *Pdgfc* expression would be further elevated in 18–24-month-'old' mice. In addition to *Pdgfc*, we show upregulation of fibroblast activation and fibrosis genes in aged mouse lungs, and, importantly, for the majority of these, including *Pdgfc* and *Plat*, expression is further enhanced in TB lungs, supporting the positive feedback loop between tumor cells and the activated microenvironment. Although macrophages as well as fibroblasts and tumor cells contribute to this upregulation of *Pdgfc* expression in TB aged lungs, our findings are recapitulated in a dormancy model using human ER$^+$ ZR-75-1 cells in immunocompromised mice, indicating that PDGF-C can elicit its pro-metastatic effects in an immune-independent manner.

Using syngeneic models of ER$^+$ breast cancer in young and aged mice reveals a previously unappreciated role of PDGF-C in ER$^+$ breast cancer metastasis and the utility of targeting PDGFRα with imatinib, a drug that is a well-tolerated, clinically relevant therapeutic agent with an equivalent efficacy and safety profile in old and young patients with chronic myeloid leukemia[40,41] and can reduce bleomycin-induced fibrosis[42]. Importantly, given that imatinib additionally targets other tyrosine kinases such as KIT, CSF1R and BCR–ABL[43], our findings are recapitulated using a PDGF-C-blocking antibody. Together, these data reinforce a growing body of evidence describing the role of the metastatic microenvironment in regulating DTC outgrowth[44–46] and support a model in which the PDGF-C^{hi} microenvironment supports

https://doi.org/10.1038/s43018-023-00525-y

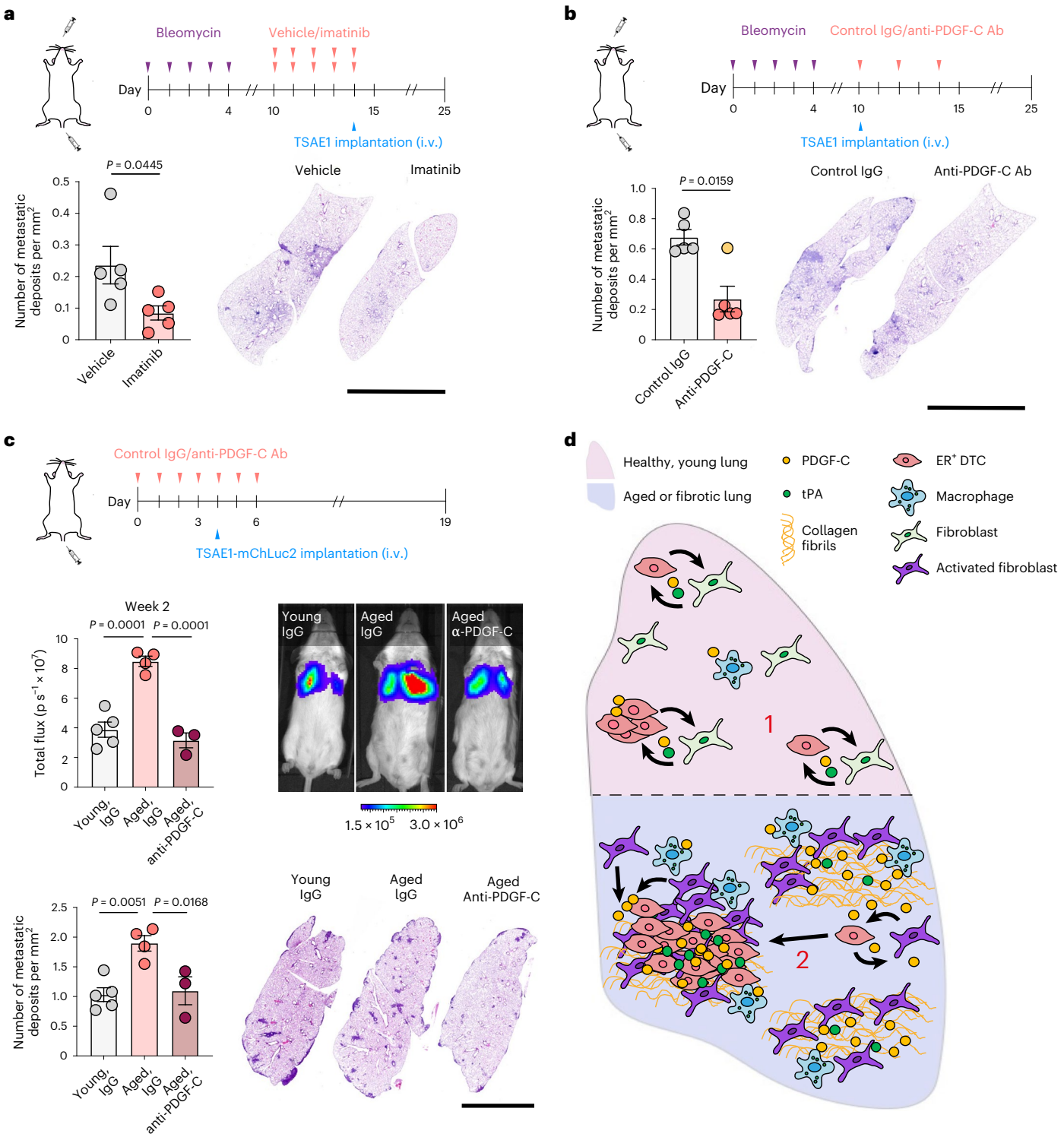

Fig. 8 | Inhibition of PDGF-C signaling in the aged or fibrotic microenvironment limits metastatic outgrowth of ER$^+$ tumor cells. a,**b**, Young mice were pretreated with bleomycin and then received either vehicle or imatinib (**a**) or immunoglobulin (Ig)G control or anti-PDGF-C antibody (Ab) (**b**), as indicated ($n = 5$ mice per group). Mice were injected intravenously with TSAE1 cells on day 14 (**a**) or day 10 (**b**), and experiments ended on day 25. The number of lung metastatic deposits was quantified, with representative lung sections shown (scale bar, 5 mm). For **b**, an outlier was identified (yellow circle) using the outlier analysis in GraphPad Prism (ROUT method, $q = 1\%$). The P value shown excludes the outlier ($P = 0.0556$ with the outlier included). **c**, Aged (>12-month-old) BALB/c mice were treated with control IgG ($n = 4$ mice) or PDGF-C-blocking antibody ($n = 3$ mice) as indicated. Young mice ($n = 5$ mice) were treated with control antibody. Middle, IVIS signal at week 2 after tumor cell injection, with representative whole-body IVIS images (scale bar, radiance, p s^{-1} cm^{-2} sr^{-1}). Bottom, number of lung metastatic deposits, with representative lung sections (scale bar, 5 mm). **d**, Proposed model for PDGF-C in ER$^+$ breast cancer metastatic relapse. (1) Single ER$^+$ DTCs have low-level *PDGFC* expression, which aids DTC survival but is insufficient for the generation of a metastasis-permissive niche. (2) An activated PDGF-C^{hi} stroma in aged or fibrotic lungs supports proliferation of PDGF-C^{lo}ER$^+$ DTCs, with levels of PDGF-C (tumor and stroma derived) and its activator tPA elevated in the growing lesions, further activating fibroblasts and supporting the development of macrometastatic lesions. Data are presented as mean values ± s.e.m.; two-tailed t-test (**a**), two-tailed Mann–Whitney U-test (**b**) or one-way ANOVA with multiple comparisons (**c**).

rapid metastatic outgrowth in aged mice or mice with lung fibrosis by acting to recruit and activate PDGFRα-positive fibroblasts and increase tPA levels, required for proteolytic cleavage of the PDGF-C precursor. By contrast, the low level of PDGF-C in young healthy lungs is insufficient to create a pro-metastatic microenvironment to support ER^+ DTC outgrowth. Instead, DTC survival and outgrowth is dependent upon tumor cell-derived PDGF-C. However, it is likely that, in the clinical scenario of single ER^+ DTCs lodged at secondary sites, as modeled here in spontaneous metastasis assays, the level of PDGF-C produced is insufficient to generate robust tumor cell–stromal cross-talk and creation of a productive metastatic niche, delaying metastatic outgrowth until these age-related changes at secondary sites trigger ER^+ DTCs to reawaken.

Methods

In vivo studies

All animal work was carried out under UK Home Office Project licenses P6AB1448A and PP4856884 (establishment license X702B0E74) and was approved by the 'Animal Welfare and Ethical Review Body' at the Institute of Cancer Research and Imperial College London. Female BALB/c, FVB/NCrl, C57BL/6 and NSG mice were from Charles River. Young mice were 8–10 weeks old at the start of the experiment. Aged mice were aged in house or were from Charles River and were 9–18 months old at the start of the experiment (figure legends). Aged mice were closely monitored for signs of frailty. All NSG mice and, where indicated, BALB/c and FVB mice were implanted with a slow-release 17β-estradiol pellet (NE-121, 0.36 mg, 90 d; Innovative Research of America) subcutaneously 3–5 d before inoculation with tumor cells. In all cases, experiments were terminated if a mouse showed signs of ill health or lost 20% of its body weight over 72 h or if the primary tumor (unilateral) reached a mean diameter of >17 mm. The maximum tumor size permitted by the license (mean diameter, 18 mm) was not breached.

Orthotopic inoculation. A total of 2×10^5 TSAE1, EMT6, 4T1 or D2A1 cells or 2×10^6 ZR-75-1-mChLuc2 cells were injected into the fourth mammary fat pad of mice under general anesthesia. Cells were injected in sterile PBS, except EMT6 cells, which were injected in 1:1 growth factor-reduced Matrigel (Corning, 356231):PBS. Tumor growth was measured biweekly, and tumor volume was calculated using the formula volume = (length × width^2) ÷ 2.

Intravenous inoculation. A total of $3–10 \times 10^4$ TSAE1 or HRM1 cells, 5×10^5 AT-3 cells or 3×10^6 ZR-75-1-mChLuc2 cells were injected into the lateral tail vein. Mice were culled when the first mouse showed signs of metastatic disease, except for Fig. 2k, for which the experiment was ended earlier. When indicated, $5–8 \times 10^5$ CAFs were injected intravenously 3 and 8 d following TSAE1 inoculation.

Treatments. Mice were treated with 0.1 mg per kg (NSG) or 0.25 mg per kg (BALB/c) bleomycin sulfate (Sigma, 203401) in 0.9% NaCl intranasally once daily for 5 d. BALB/c mice were dosed with 50 mg per kg imatinib mesylate (Sigma) or vehicle (water) twice daily intraperitoneally. NSG mice were dosed twice daily with 25 mg per kg imatinib mesylate or vehicle for 7 d and then 37.5 mg per kg twice daily for 2 weeks. For treatment with anti-PDGF-C-blocking antibody or normal goat IgG control, mice received 20 µg antibody in 0.9% NaCl intranasally (30 µl per nostril) every other day for three doses (Fig. 8b) or once daily for 7 d (Fig. 8c). For rPDGF-C treatment, 3 µg per 20 g mouse body weight was administered intranasally (30 µl per nostril in 0.9% NaCl) once daily for 5 d.

IVIS imaging. Mice were injected intraperitoneally with 150 mg per kg D-luciferin (Caliper Life Sciences) and imaged in vivo, or organs were imaged ex vivo 5 min after injection (IVIS Lumina II). Luminescence was quantified as total counts, for which imaging settings and time were kept constant, or as total flux (p s^{-1}). Analysis was performed (Living Image Software, PerkinElmer, 4.7.3) maintaining the region of interest over the tissues as a constant size.

Quantification of metastatic burden. Two 3–4-µm lung or liver FFPE sections were cut 150–200 µm apart, H&E stained and scanned (NanoZoomer Digital Pathology (NDP), Hamamatsu). Metastatic deposits were counted (two sections per animal), with file names blinded (NDP.view2, 2.7.52). For syngeneic experiments, deposits were counted, if visible, on the H&E sections. For experiments with ZR-75-1 cells, deposits were defined when >5 human lamin A/C-positive cells were present in a cluster. For quantification of ZR-75-1 single DTCs, human lamin A/C-positive cells were counted excluding those in metastatic deposits (clusters of >5 cells). Lung or liver metastatic area was calculated manually or using Fiji (ImageJ, 2.0.0-rc-54/1.51h).

Immunofluorescence and immunohistochemistry. Immunohistochemical staining was performed as indicated, with detection via VECTASTAIN ABS. For immunofluorescence, 3–4-µm FFPE sections were rehydrated, antigen-retrieved (DAKO Target Retrieval Solution) and blocked in PBS (1% BSA and 2% FBS) before incubating with primary antibody overnight at 4 °C and secondary antibodies for 40 min at room temperature. Sections were scanned using NDP (low-power images). High-power images were taken with the Lecia SP8 confocal microscope. The level of gamma correction was adjusted for images on NDP and kept consistent between panels.

EdU-incorporation assays. EdU assays were performed as previously described[8] using the Click-iT Plus EdU kit (Thermo Fisher Scientific, C10637). In brief, 24 h before culling, mice were injected intraperitoneally with 200 µl EdU (Thermo Fisher Scientific, E10187) solution (20 mg ml^{-1} in 0.9% NaCl). EdU^+ tumor cells were identified in frozen sections by counterstaining with human lamin A/C (Fig. 6d) or in FFPE sections using an antibody against HMGA2 (Fig. 2b). A minimum of six images were quantified from frozen sections, or the total number EdU^+ tumor cells was quantified in FFPE sections of one mouse lung lobe. *Hmga2* was identified as a marker to detect TSAE1 cells in the lung as it is highly expressed in TSAE1 cells (8.6 $\log_2$ (CPM) from RNA-seq data associated with Fig. 1a,b) but not expressed in the normal mouse lung (−2.4 $\log_2$ (CPM) mean expression in NTB samples from RNA-seq data from Fig. 2d), with subsequent validation of TSAE1 staining performed on tumor and lung sections.

RNAscope. Freshly cut 5-µm sections were used for RNAscope. IHC–ISH for α-SMA and *Pdgfc* (Mm-Pdgfc-No-XHs, ACD, 441559) was performed using the sequential co-detection workflow, or ISH was performed alone for *PDGFC* (Hs-PDGFC-No-XMm, ACD, 442919) on the Ventana DISCOVERY ULTRA (VSS version 12.5.4) with reagents from Roche and ACD (Bio-Techne) according to the manufacturer's instructions for the RNAscope VS Universal HRP kit (ACD, 323200). A 24-min cell conditioning step and a 48-min AMP5 step were used. Control probes used were negative control (*dapB*, ACD, 312039) and positive control (human, VS probe Hs-PPIB-No-XMm, ACD, 844229; mouse, VS Probe Mm-Ppib-No-XHs, ACD, 844239). Sections were counterstained with hematoxylin and scanned on NDP.

Tumor cell isolation and fluorescence-activated cell sorting. Tumors and lungs were dissociated using the mouse tumor or lung dissociation kit (Miltenyi Biotec, 130-096-730 or 130-095-927), collected in Buffer S and dissociated into single-cell suspensions using the gentleMACS Octo Dissociator (Miltenyi) and the program 37C_m_TDK_2 or 37C_m_LDK_1, respectively. For isolating tumor cells, single-cell suspensions were stained with DAPI to exclude dead cells, and $mCherry^+$ cells were sorted on a FACSAria III Cell Sorter directly into lysis buffer

for RNA extraction using the RNeasy micro plus kit (Qiagen; Fig. 3g,h), or 1,000 ZR-75-1-mChLuc2 cells were plated per well in a 96-well plate (Fig. 6a). For isolating cell populations from aged mice (Extended Data Fig. 4c) and sorting mCherry$^+$ tumor cells from young or aged TB mice (Fig. 3i), lungs were dissociated as described above into single-cell suspensions, and red blood cell lysis was performed (BD Biosciences, 555899) followed by an FC block. Cells were stained for CD45, CD31, EpCAM, PDGFRα, F4/80 and DAPI for sorting different cell populations or CD45, CD31 and DAPI to exclude immune cells, endothelial cells and dead cells, respectively. Cells were sorted on a BD Symphony S6 cell sorter directly into lysis buffer as described above, with compensation controls set up using UltraComp eBeads (eBioscience, 01-2222-42). SH800 and BD FACSDiva (8.0.1) software was used. Example gating strategies are shown in Supplementary Figs. 1 and 2.

Reagents and cells

Antibodies and dilutions used are detailed in Supplementary Table 1. Human rPDGF-C was from Sigma (SRP3139). TSAE1 (TS/A-E1)[47], HRM1 (ref. [48]), EMT6 (ref. [49]) and F3II[50] cells were obtained from L. Wakefield[12] (National Cancer Institute, USA) with permission of C. De Giovanni, J. Zhao, S. Rockwell and D. Alonso, respectively. D2A1 and D2.OR cells were from A. Chambers' laboratory stocks[51] (London Health Sciences Centre, Canada). D2A1-m1 and D2A1-m2 metastatic sublines were generated in house[13]. ZR-75-1 (CRL-1500), 10T1/2 (CCL-226), 3T3 (CRL-1658), 4T1 (CRL-2539), IMR90 (CCL-186), MRC5 (CCL-171) and HEK293T (CRL-3216) cells were from ATCC. AT-3 cells were provided by C. Paget and D. Soulard (Institute Pasteur de Lille). GFP-positive CAFs were from 4T1-TB BALB/c Ub-GFP mice[52]. Young (BALB-5013 and C57-6013) and aged (A57-6013, two independent batches from 58–78-week-old mice) mouse primary lung fibroblasts (Cell Biologics) were cultured in fibroblast medium (M2267, Cell Biologics) until immortalized (see below), after which they were cultured in DMEM (10% FBS). All other cells were maintained in DMEM (10% FBS) unless otherwise stated. All cells were routinely checked for mycoplasma contamination (MycoAlert, Lonza). The identity of ZR-75-1 cells was confirmed by short tandem repeat (GenePrint 10 System, Promega).

In vitro studies

***Greb1* expression.** Cells were cultured in phenol red-free DMEM (10% FBS) for >72 h before seeding. The following day, cells were treated with 4-OHT (Sigma, H7904) in phenol red-free medium (10% FBS). After 18 h, treatments were refreshed, and cells were collected for RNA extraction 6 h later.

CellTiter-Glo assays. Cells were seeded at 500 (mouse tumor lines) or 2,000 (fibroblasts or ZR-75-1 tumor cells) cells per well in 96-well plates. For rPDGF-C treatment, cells were serum starved the following day for 6 h before being treated with vehicle or 100 ng ml^{-1} rPDGF-C in serum-free DMEM (SFM) for 48 or 72 h. For imatinib treatment, the following day, cells were treated with vehicle or 1 µM imatinib mesylate for 72 h. Cell viability was analyzed by CellTiter-Glo (Promega) at the indicated time points.

Colony-formation assays. Cells were cultured in phenol red-free DMEM (10% FBS) for >72 h before seeding. A total of 10,000 cells were seeded in 100 µl 1:1 Matrigel (356237):phenol red-free DMEM (10% FBS). One milliliter of phenol red-free DMEM (10% FBS) was added with vehicle, 4-OHT or fulvestrant (Sigma, 14409) at the indicated concentrations in duplicate. For charcoal-stripped conditions, cells were seeded in and subsequently treated with phenol red-free DMEM with 10% charcoal-stripped FBS (Gibco, 12676029). Treatments were refreshed on day 4 after seeding. On day 7, a minimum of three images were taken per well (six wells per treatment group). Colony size was calculated using ImageJ.

Dormancy and reactivation assays. Cells were seeded at 100 (mouse lines) or 1,000 (ZR-75-1) cells per well in six-well plates in DMEM (10% FBS). The following day, the medium was changed to dormancy medium (DMEM plus 2% FBS, 4.5 g l^{-1} glucose for ZR-75-1 cells and 1 g l^{-1} glucose for mouse tumor cells). After 7–10 d, multiple images were taken per well on the EVOS microscope, and wells were stained with crystal violet. The remaining wells were refreshed with dormancy medium or treated with DMEM or CM plus 5% FBS. Seven to 10 d later, wells were stained and imaged. For generation of CM, tumor cells or fibroblasts were grown to 70–80% confluency, washed once and cultured in SFM. CM was collected 24 h later, centrifuged at 300*g* and filtered through a 0.2-µm filter. CM was supplemented with FBS after collection as indicated. For soft agar assays, 1.5 ml of 1:1 1% agar:medium (10% FBS) was plated per well of a six-well plate and allowed to set. A total of 5,000 cells were seeded in 1.5 ml of 1:1 0.6% agar:medium (10% FBS). Every 3–4 d, 200 µl medium was added. After 6 weeks, live cells were stained with 4 µM calcein AM for 1 h at room temperature and imaged on an EVOS microscope. BME assays were performed as described previously[4], with 800 tumor cells seeded per well in a 96-well plate or 2,000 cells in a chamber slide well, or, for co-cultures, with the addition of 1,000 or 2,500 fibroblasts, respectively. Immortalized primary lung fibroblasts were used (see below). Images were taken every 3–4 d for 3 weeks. For DiD staining, 1×10^6 tumor cells were incubated at 37 °C for 20 min in the dark with 5 µl Vybrant DiD Cell-Labeling Solution (Thermo Fisher Scientific, V22887) in 1 ml SFM, washed and seeded in the BME assays as described above. For proliferative controls, 8,000 (96-well) or 20,000 (chamber slide well) DiD-labeled tumor cells were seeded. For the experiment shown in Fig. 6a, ZR-75-1-mChLuc2 cells isolated from lungs were cultured in DMEM (10% FBS) for 3 d, before the medium was changed to fresh DMEM (5% FBS) or 4T1, 3T3 or MRC5 CM supplemented with 5% FBS. Images were taken after 7 and 14 d, and the number of tumor cells in each colony was counted.

Viral production and infection. shRNA plasmids were purified from MISSION TRC shRNA bacterial glycerol stocks (Sigma; Supplementary Table 2). The PGK-H2BmCherry-IRES-Luc2 plasmid was used for the generation of mChLuc2-tagged cell lines[52]. The EX-Mm07346-Lv185 *Pdgfc* plasmid and empty control vector (EV; EX-NEG-Lv185) were from GeneCopoeia. All plasmids were packaged using HEK293T cells and helper plasmids pRRE, pREV and pVsV-G using standard protocols. Viral medium was collected 48 h after transfection, and target cells were infected with the viral medium supplemented with 8 µg ml^{-1} polybrene. Primary lung fibroblasts were immortalized using an HPV-16 E6/E7 lentivirus (1×10^6 IU ml^{-1}, NBS Biologicals, G268; EF1α promoter). Virus-containing medium was added at a 1:1 dilution with medium to fibroblasts and incubated with 8 µg ml^{-1} polybrene for 48 h. All transduced cells were subsequently selected with puromycin (stable knockdown or overexpression lines) or G418 (fibroblasts) or by sorting for mCherry$^+$ cells (mChLuc2 cell lines).

Western blotting. Cells were serum starved overnight and then pretreated with vehicle or imatinib mesylate (1 µM) for 1 h in SFM before being treated with vehicle or 100 ng ml^{-1} rPDGF-C in the presence of vehicle or 1 µM imatinib mesylate for 30 min (SFM). Cells were lysed in RIPA buffer (Sigma), and blots were blocked with 5% milk before incubation with antibodies. Blots were imaged and analyzed on a ChemiDoc System with Image Lab (Bio-Rad, 6.1).

Quantitative PCR with reverse transcription

Pdgfc expression was assessed in primary lung fibroblasts before immortalization. Lungs or tumors were homogenized in lysis buffer using a Precellys tissue homogenizer. RNA was isolated using Qiagen RNeasy Plus Micro (homogenized tissues) or RNeasy Plus Mini (cells) kits. cDNA was generated using the QuantiTect reverse transcriptase kit (Qiagen) or the SuperScript IV kit (Invitrogen) with random hexamers

for overexpression lines. RT–qPCR was performed with Taqman Gene Expression Assay probes (Supplementary Table 3) on a QuantStudio 6 Flex Real-Time PCR System (Applied Biosystems, 1.7.1). Each reaction was performed in triplicate, and relative expression levels were normalized to *B2m* or *B2M* and/or *Ipo8* or *IPO8*. When calculating the relative expression across independent cell lines, multiple house-keeping genes were used (*B2m*, *Ipo8*, *Ubc* and *18s*).

RNA-seq

RNA was isolated from mouse mammary tumor cell lines or rPDGF-C- or vehicle-treated MRC5 fibroblasts or from the right lung of mice using the Qiagen RNeasy kit. Quality and quantity of the RNA was assessed using a Bioanalyzer and Qubit. Sequencing was performed using the Illumina HiSeq 4000 (in vivo RNA-seq) or the NovaSeq 6000 (RNA-seq of cell lines). RNA-seq generated 13.7–111 million reads per sample. Library quality was evaluated using FastQC (version 0.11.4), and initial bioinformatic analysis and data normalization were performed as previously described[52].

For expression analysis of mouse mammary tumor cells in vitro (Fig. 1), genes with $|\log_2(\text{fold change})| > 0.585$ and P value < 0.05 between ER^+ (TSAE1, HRM1 and EMT6) and ER^- (D2A1, D2A1-m1 and D2A1-m2 and F3II) cell lines were considered statistically significant. Analysis of differentially expressed genes ($P < 0.05$) in ER^+ versus ER^- cell lines was performed with Ingenuity Pathway Analysis (version 01-20-04), and heatmaps were generated with MeV (4.8.1). Gene set enrichment analysis (GSEA 4.1.0) was performed on ER^- (D2A1, D2A1-m1 and D2A1-m2) and ER^+ (TSAE1, HRM1 and EMT6) groups with a minimum gene set size of 15 genes and 1,000 permutations. Pathways with a normalized enrichment score (NES) > 0 and P value < 0.05 were considered upregulated, and those with NES < 0 and P value < 0.05 were considered downregulated. For RNA-seq analysis of young and aged mouse lungs (Figs. 2d,g and 3a,b), principal-component analysis was performed using R packages FactoMineR (version 2.4) and factoextra (version 1.0.7). The TSAE1 tumor signature (Supplementary Table 4) comprises a list of 33 genes that are not expressed in normal NTB mouse lungs (average $\log_2$ (CPM) < −2) but are expressed by TSAE1 cells in vitro (average $\log_2$ (CPM) > 2.9) as well as *Krt14* and *Krt16*, which exhibit the same pattern and are used to assess malignant cells in bulk tissue[53]. The fibroblast-activation signature (151 genes; Supplementary Table 5) was compiled from genes in fibroblast-activation, -proliferation and -migration signatures from the Molecular Signatures Database (GSEA; downloaded January 2021), in addition to fibroblast-activation markers *Acta2*, *S100a4* and *Fap*. The fibrosis signature (Supplementary Table 6) comprises 75 genes present in two or more of four published fibrosis datasets and the mouse Fibrosis V2 Panel (NanoString)[54–56]. Signature scores were estimated using the singular value decompositions on scaled data of constituent genes in each signature.

For PDGF-C response genes, initial analysis was performed as described above. Reads were trimmed using trim-galore version 0.6.6 and aligned to human genome assembly GRCh38 using STAR aligner version 2.7.6a. Raw counts were normalized using the R package edgeR's (version 3.28.1) TMM (trimmed mean of M values) method in the R statistical programming environment (version 3.6.0). Low-abundance genes were removed using edgeR's function 'filterByExpr()'. Differential mRNA-abundance analysis was performed using the model: '~0 + group' followed by edgeR's quasi-likelihood F-test. Analysis focused on 1,903 genes predicted to have a secreted protein product (the Human Protein Atlas).

Human dataset analysis

For analysis of the METABRIC dataset[57,58], 1,904 human breast tumors for which ER status was known were used for the assessment of *PDGFC* expression. Plots of single-cell RNA-seq data from 26 human breast cancers[21] were generated using the Broad Institute Single Cell Portal, https://singlecell.broadinstitute.org. For further details, see Data availability.

Statistics and reproducibility

No statistical method was used to predetermine sample size, but sample sizes are similar to those previously reported[13,52,59]. Data collection and analysis were not performed blinded to the conditions of all experiments. For in vitro studies, no randomization was performed, and experiments were repeated at least twice and/or validated with independent cell lines. Representative experiments were repeated, as indicated, with similar results. Age-matched mice were randomized into control and experimental groups at the start of the experiment based on body weights, except for Fig. 2b, for which mice were matched for primary tumor size. Animal experiments were performed at least twice, with similar results observed, except for Figs. 1f, 2b,f,k, 3g–i, 4d,e,h, 6c–e, 7d and 8a–c and Extended Data Figs. 1f and 6b,d,f, which represent experiments performed once. No data were excluded from the analyses, except for Fig. 4h, in which one mouse (*Pdgfc* overexpression) did not develop a tumor due to a failed injection and therefore was excluded from metastasis analysis; Fig. 6c, in which one mouse (shNTC1) died under anesthesia during imaging before the experiment endpoint; Fig. 8b, in which a statistical outlier was identified (outlier analysis with GraphPad Prism (ROUT, $q = 1\%$); outlier is highlighted, and P values with and without outlier are indicated); Fig. 8c, in which one mouse in the aged group treated with anti-PDGF-C antibody was excluded due to failed injection.

Statistics were performed using GraphPad Prism 8 apart from pathway analysis (IPA). All comparisons between two groups were made using a two-tailed, unpaired t-test unless the analysis did not pass a normality test (Shapiro–Wilk test), in which case, a two-tailed Mann–Whitney U-test was used. Equal variances were not formally tested. When more than two groups were compared, a one-way ANOVA test was performed with Holm–Sidak's multiple-comparison test or a Kruskal–Wallis test with Dunn's multiple-comparison test if the normality test was not passed (Shapiro–Wilk test). When there were two independent variables and multiple groups, a two-way ANOVA was performed with Sidak's test for multiple comparisons or multiple t-tests for grouped analysis. Correlation analysis was performed using a two-tailed Pearson's correlation test with R^2 values shown. The box plots in Figs. 1d and 3e and Extended Data Figs. 1e and 2c show median (center line) and 25th–75th quartiles with the whiskers at minimum and maximum.

Reporting summary

Further information on research design is available in the Nature Portfolio Reporting Summary linked to this article.

Data availability

The mammary tumor cell line and young and aged lung RNA-seq datasets are deposited in the Sequence Read Archive under the accession number PRJNA822368. The dataset for RNA-seq of rPDGF-C treatment of MRC5 fibroblasts is deposited in the Sequence Read Archive under the accession number PRJNA895434. RNA-seq data from the METABRIC dataset were downloaded from cBioPortal[57,58]. RNA expression data for 57 human breast cancer cell lines were downloaded from the Broad Institute (CCLE). Non-cancerous lung gene expression data (GSE23546) and gene expression data for C57BL/6 mice treated with bleomycin (GSE40151) were downloaded from GEO. All other data supporting the findings of this study are available from the corresponding author on reasonable request. Source data are provided with this paper.

Code availability

Open-source software was used to analyze data in this study. Details of software versions and parameters are specified in relevant sections in the Methods.

References

1. Ribelles, N. et al. Pattern of recurrence of early breast cancer is different according to intrinsic subtype and proliferation index. *Breast Cancer Res.* **15**, R98 (2013).
2. Pan, H. et al. 20-year risks of breast-cancer recurrence after stopping endocrine therapy at 5 years. *N. Engl. J. Med.* **377**, 1836–1846 (2017).
3. Ghajar, C. M. et al. The perivascular niche regulates breast tumour dormancy. *Nat. Cell Biol.* **15**, 807–817 (2013).
4. Vera-Ramirez, L., Vodnala, S. K., Nini, R., Hunter, K. W. & Green, J. E. Autophagy promotes the survival of dormant breast cancer cells and metastatic tumour recurrence. *Nat. Commun.* **9**, 1944 (2018).
5. Malladi, S. et al. Metastatic latency and immune evasion through autocrine inhibition of WNT. *Cell* **165**, 45–60 (2016).
6. Albrengues, J. et al. Neutrophil extracellular traps produced during inflammation awaken dormant cancer cells in mice. *Science* **361**, eaao4227 (2018).
7. Nobre, A. R. et al. Bone marrow NG2$^+$/Nestin$^+$ mesenchymal stem cells drive DTC dormancy via TGFβ2. *Nat. Cancer* **2**, 327–339 (2021).
8. Montagner, M. et al. Crosstalk with lung epithelial cells regulates Sfrp2-mediated latency in breast cancer dissemination. *Nat. Cell Biol.* **22**, 289–296 (2020).
9. Di Martino, J. S. et al. A tumor-derived type III collagen-rich ECM niche regulates tumor cell dormancy. *Nat. Cancer* **3**, 90–107 (2022).
10. Er, E. E. et al. Pericyte-like spreading by disseminated cancer cells activates YAP and MRTF for metastatic colonization. *Nat. Cell Biol.* **20**, 966–978 (2018).
11. Lu, X. et al. VCAM-1 promotes osteolytic expansion of indolent bone micrometastasis of breast cancer by engaging α4β1-positive osteoclast progenitors. *Cancer Cell* **20**, 701–714 (2011).
12. Yang, Y. et al. Immunocompetent mouse allograft models for development of therapies to target breast cancer metastasis. *Oncotarget* **8**, 30621–30643 (2017).
13. Jungwirth, U. et al. Generation and characterisation of two D2A1 mammary cancer sublines to model spontaneous and experimental metastasis in a syngeneic BALB/c host. *Dis. Model. Mech.* **11**, dmm031740 (2018).
14. Peng, R. et al. Bleomycin induces molecular changes directly relevant to idiopathic pulmonary fibrosis: a model for "active" disease. *PLoS ONE* **8**, e59348 (2013).
15. de Vries, M. et al. Lung tissue gene-expression signature for the ageing lung in COPD. *Thorax* **73**, 609–617 (2017).
16. Folestad, E., Kunath, A. & Wagsater, D. PDGF-C and PDGF-D signaling in vascular diseases and animal models. *Mol. Aspects Med.* **62**, 1–11 (2018).
17. Fane, M. E. et al. Stromal changes in the aged lung induce an emergence from melanoma dormancy. *Nature* **606**, 396–405 (2022).
18. Travaglini, K. J. et al. A molecular cell atlas of the human lung from single-cell RNA sequencing. *Nature* **587**, 619–625 (2020).
19. Anderberg, C. et al. Paracrine signaling by platelet-derived growth factor-CC promotes tumor growth by recruitment of cancer-associated fibroblasts. *Cancer Res.* **69**, 369–378 (2009).
20. Roswall, P. et al. Microenvironmental control of breast cancer subtype elicited through paracrine platelet-derived growth factor-CC signaling. *Nat. Med.* **24**, 463–473 (2018).
21. Wu, S. Z. et al. A single-cell and spatially resolved atlas of human breast cancers. *Nat. Genet.* **53**, 1334–1347 (2021).
22. Eitner, F. et al. PDGF-C is a proinflammatory cytokine that mediates renal interstitial fibrosis. *J. Am. Soc. Nephrol.* **19**, 281–289 (2008).
23. Gilbertson, D. G. et al. Platelet-derived growth factor C (PDGF-C), a novel growth factor that binds to PDGF α and β receptor. *J. Biol. Chem.* **276**, 27406–27414 (2001).
24. Hurst, N. J. Jr., Najy, A. J., Ustach, C. V., Movilla, L. & Kim, H. R. Platelet-derived growth factor-C (PDGF-C) activation by serine proteases: implications for breast cancer progression. *Biochem. J.* **441**, 909–918 (2012).
25. Opzoomer, J. W. et al. Macrophages orchestrate the expansion of a proangiogenic perivascular niche during cancer progression. *Sci. Adv.* **7**, eabg9518 (2021).
26. Shook, B. A. et al. Myofibroblast proliferation and heterogeneity are supported by macrophages during skin repair. *Science* **362**, eaar2971 (2018).
27. Chandler, C., Liu, T., Buckanovich, R. & Coffman, L. G. The double edge sword of fibrosis in cancer. *Transl. Res.* **209**, 55–67 (2019).
28. Andrae, J., Gallini, R. & Betsholtz, C. Role of platelet-derived growth factors in physiology and medicine. *Genes Dev.* **22**, 1276–1312 (2008).
29. Heldin, C. H., Lennartsson, J. & Westermark, B. Involvement of platelet-derived growth factor ligands and receptors in tumorigenesis. *J. Intern. Med.* **283**, 16–44 (2018).
30. MacParland, S. A. et al. Single cell RNA sequencing of human liver reveals distinct intrahepatic macrophage populations. *Nat. Commun.* **9**, 4383 (2018).
31. Crawford, Y. et al. PDGF-C mediates the angiogenic and tumorigenic properties of fibroblasts associated with tumors refractory to anti-VEGF treatment. *Cancer Cell* **15**, 21–34 (2009).
32. Yoon, H. et al. Cancer-associated fibroblast secretion of PDGFC promotes gastrointestinal stromal tumor growth and metastasis. *Oncogene* **40**, 1957–1973 (2021).
33. Bartoschek, M. & Pietras, K. PDGF family function and prognostic value in tumor biology. *Biochem. Biophys. Res. Commun.* **503**, 984–990 (2018).
34. Bandapalli, O. R., Macher-Goeppinger, S., Schirmacher, P. & Brand, K. Paracrine signalling in colorectal liver metastases involving tumor cell-derived PDGF-C and hepatic stellate cell-derived PAK-2. *Clin. Exp. Metastasis* **29**, 409–417 (2012).
35. Liedtke, C. et al. The prognostic impact of age in different molecular subtypes of breast cancer. *Breast Cancer Res. Treat.* **152**, 667–673 (2015).
36. Marsh, T. et al. Hematopoietic age at onset of triple-negative breast cancer dictates disease aggressiveness and progression. *Cancer Res.* **76**, 2932–2943 (2016).
37. Fane, M. & Weeraratna, A. T. How the ageing microenvironment influences tumour progression. *Nat. Rev. Cancer* **20**, 89–106 (2020).
38. Borriello, L. et al. Primary tumor associated macrophages activate programs of invasion and dormancy in disseminating tumor cells. *Nat. Commun.* **13**, 626 (2022).
39. Kaur, A. et al. sFRP2 in the aged microenvironment drives melanoma metastasis and therapy resistance. *Nature* **532**, 250–254 (2016).
40. Gugliotta, G. et al. Frontline imatinib treatment of chronic myeloid leukemia: no impact of age on outcome, a survey by the GIMEMA CML Working Party. *Blood* **117**, 5591–5599 (2011).
41. Sanchez-Guijo, F. M. et al. Evaluation of tolerability and efficacy of imatinib mesylate in elderly patients with chronic phase CML: ELDERGLI study. *Leuk. Res.* **35**, 1184–1187 (2011).
42. Aono, Y. et al. Imatinib as a novel antifibrotic agent in bleomycin-induced pulmonary fibrosis in mice. *Am. J. Respir. Crit. Care Med.* **171**, 1279–1285 (2005).
43. Zitvogel, L., Rusakiewicz, S., Routy, B., Ayyoub, M. & Kroemer, G. Immunological off-target effects of imatinib. *Nat. Rev. Clin. Oncol.* **13**, 431–446 (2016).

44. Linde, N., Fluegen, G. & Aguirre-Ghiso, J. A. The relationship between dormant cancer cells and their microenvironment. *Adv. Cancer Res.* **132**, 45–71 (2016).
45. Lim, A. R. & Ghajar, C. M. Thorny ground, rocky soil: tissue-specific mechanisms of tumor dormancy and relapse. *Semin. Cancer Biol.* **78**, 104–123 (2022).
46. Massague, J. & Ganesh, K. Metastasis-initiating cells and ecosystems. *Cancer Discov.* **11**, 971–994 (2021).
47. Lollini, P. L. et al. High-metastatic clones selected in vitro from a recent spontaneous BALB/c mammary adenocarcinoma cell line. *Clin. Exp. Metastasis* **2**, 251–259 (1984).
48. Liu, P. et al. Oncogenic PIK3CA-driven mammary tumors frequently recur via PI3K pathway-dependent and PI3K pathway-independent mechanisms. *Nat. Med.* **17**, 1116–1120 (2011).
49. Rockwell, S. C., Kallman, R. F. & Fajardo, L. F. Characteristics of a serially transplanted mouse mammary tumor and its tissue-culture-adapted derivative. *J. Natl Cancer Inst.* **49**, 735–749 (1972).
50. Alonso, D. F. et al. Characterization of F3II, a sarcomatoid mammary carcinoma cell line originated from a clonal subpopulation of a mouse adenocarcinoma. *J. Surg. Oncol.* **62**, 288–297 (1996).
51. Morris, V. L., Tuck, A. B., Wilson, S. M., Percy, D. & Chambers, A. F. Tumor progression and metastasis in murine D2 hyperplastic alveolar nodule mammary tumor cell lines. *Clin. Exp. Metastasis* **11**, 103–112 (1993).
52. Jungwirth, U. et al. Impairment of a distinct cancer-associated fibroblast population limits tumour growth and metastasis. *Nat. Commun.* **12**, 3516 (2021).
53. Yu, X., Chen, Y. A., Conejo-Garcia, J. R., Chung, C. H. & Wang, X. Estimation of immune cell content in tumor using single-cell RNA-seq reference data. *BMC Cancer* **19**, 715 (2019).
54. Bauer, Y. et al. A novel genomic signature with translational significance for human idiopathic pulmonary fibrosis. *Am. J. Respir. Cell Mol. Biol.* **52**, 217–231 (2015).
55. Cabrera, S. et al. Gene expression profiles reveal molecular mechanisms involved in the progression and resolution of bleomycin-induced lung fibrosis. *Am. J. Physiol. Lung Cell. Mol. Physiol.* **304**, L593–L601 (2013).
56. Gangwar, I. et al. Detecting the molecular system signatures of idiopathic pulmonary fibrosis through integrated genomic analysis. *Sci. Rep.* **7**, 1554 (2017).
57. Pereira, B. et al. The somatic mutation profiles of 2,433 breast cancers refines their genomic and transcriptomic landscapes. *Nat. Commun.* **7**, 11479 (2016).
58. Rueda, O. M. et al. Dynamics of breast-cancer relapse reveal late-recurring ER-positive genomic subgroups. *Nature* **567**, 399–404 (2019).
59. Jenkins, L. et al. Cancer-associated fibroblasts suppress $CD8^+$ T-cell infiltration and confer resistance to immune-checkpoint blockade. *Cancer Res.* **82**, 2904–2917 (2022).

Acknowledgements

This work was funded by program grants from Breast Cancer Now as part of program funding to the Breast Cancer Now Toby Robins Research Centre (C.M.I., S.H.). We thank Breast Cancer Now, working in partnership with Walk the Walk for supporting the work of S.H. This work represents independent research supported by the National Institute for Health Research Biomedical Research Centre at the Royal Marsden NHS Foundation Trust and the Institute of Cancer Research, London. The views expressed are those of the authors and not necessarily those of the National Institute for Health Research or the Department of Health and Social Care. We thank L. Wakefield for her help and insight on ER^+ cell line characterization and C. De Giovanni, J. Zhao, S. Rockwell and D. Alonso for permission to use the ER^+ lines; U. Jungwirth and L. O'Leary for helpful discussions regarding D2A1 sublines and in vitro dormancy assays, respectively; S. Lawson and J. Alexander in S.H.'s team for contributing to the bioinformatic analysis and E. Sahai and S. Hooper for guidance on the EdU assay; D. Vicente for help with in vivo studies and R. Evans, L. Jenkins and H. Ale for their advice in designing the cell-sorting experiments. We thank the ICR and Imperial College Biological Services Units for support with animal work, the ICR Tumour Profiling Unit for performing RNA-seq on cell lines, the ICR FACS and Light Microscopy Facility for help with cell sorting, I. Roxanis and the Breast Cancer Now Toby Robins Research Centre Nina Barough Pathology Core Facility for histopathology support and Breast Cancer Now, working in partnership with Walk the Walk, for supporting the work of the pathology team.

Author contributions

Conceptualization: F.K.T. and C.M.I. Data curation: A.G. and S.H. Supervision: F.K.T., S.H. and C.M.I. Funding acquisition: C.M.I. Investigation: F.K.T., R.O., N.J.G., A.G., M.G., C.S., S.H. and C.M.I. Writing of the original draft: F.K.T. and C.M.I. Writing (review and editing): F.K.T., R.O., S.H. and C.M.I.

Competing interests

The authors declare no competing interests.

Additional information

Extended data is available for this paper at https://doi.org/10.1038/s43018-023-00525-y.

Supplementary information The online version contains supplementary material available at https://doi.org/10.1038/s43018-023-00525-y.

Correspondence and requests for materials should be addressed to Clare M. Isacke.

Peer review information *Nature Cancer* thanks Ana Gomes, Roger Gomis and the other, anonymous, reviewer(s) for their contribution to the peer review of this work.

https://doi.org/10.1038/s43018-023-00525-y

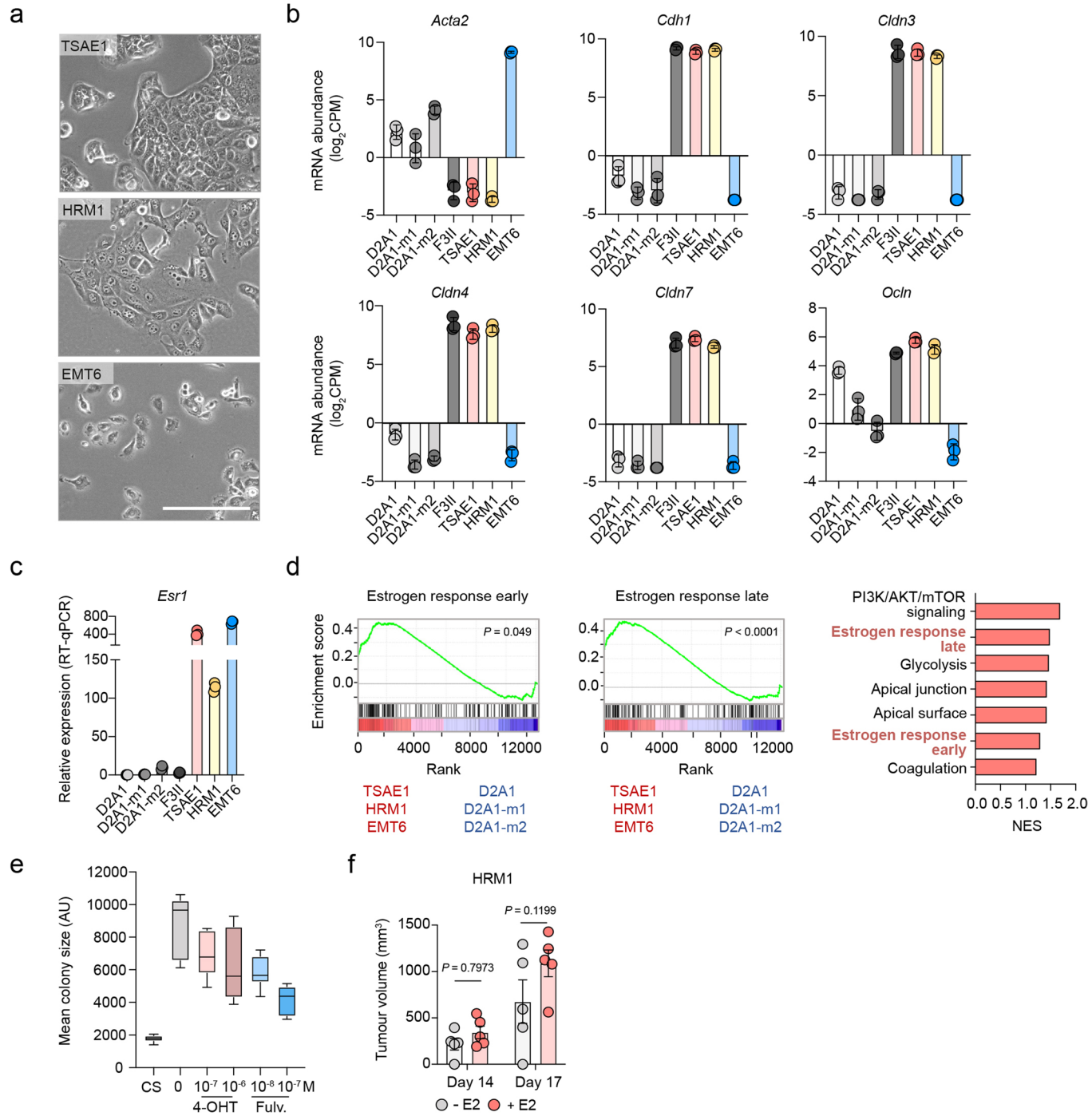

Extended Data Fig. 1 | Characterisation of ER$^+$ mouse mammary tumour cell lines. a, Phase contrast images of TSAE1, HRM1 and EMT6 cells in 2D culture (scale bar, 200 µm). **b**, Expression of *Acta2, Cdh1* and claudin genes in mouse mammary tumour lines from Fig. 1b. RNA-seq analysis (log_2CPM). **c**, *Esr1* expression (RT-qPCR) in mouse mammary tumour cell lines with normalisation performed using average expression of four house-keeping genes (*B2m*, *Ipo8*, *18s* and *Ubc*). Representative data of four independent repeats. **d**, Associated with Fig. 1b. Left, GSEA enrichment plots for 'Estrogen response early' and 'Estrogen response late' genes comparing ER$^+$ (TSAE1, HRM1, EMT6) lines (red) to ER- (D2A1, D2A1-m1, D2A1-m2) lines (blue). Right, GSEA pathways significantly ($P < 0.05$) upregulated in ER$^+$ compared with ER- cell lines. NES, normalised enrichment score. **e**, Associated with Fig. 1d. Mean HRM1 colony size per well ($n = 6$ wells per condition) in Matrigel following treatment with vehicle, 4-OHT or fulvestrant (fulv.) for 7 days in phenol red-free media or in media with charcoal-stripped (CS) FBS. Representative data of two independent repeats. **f**, Associated with Fig. 1f. HRM1 cells were injected orthotopically into untreated FVB mice or mice implanted with slow release E2 pellets ($n = 5$ mice per group). **b,c,f**, Data are presented as mean values; **b**, ±SD; **f**, ±SEM, two-way ANOVA; **e**, box plot shows 25th/75th percentiles, median (line) and minimum/maximum values (whiskers).

https://doi.org/10.1038/s43018-023-00525-y

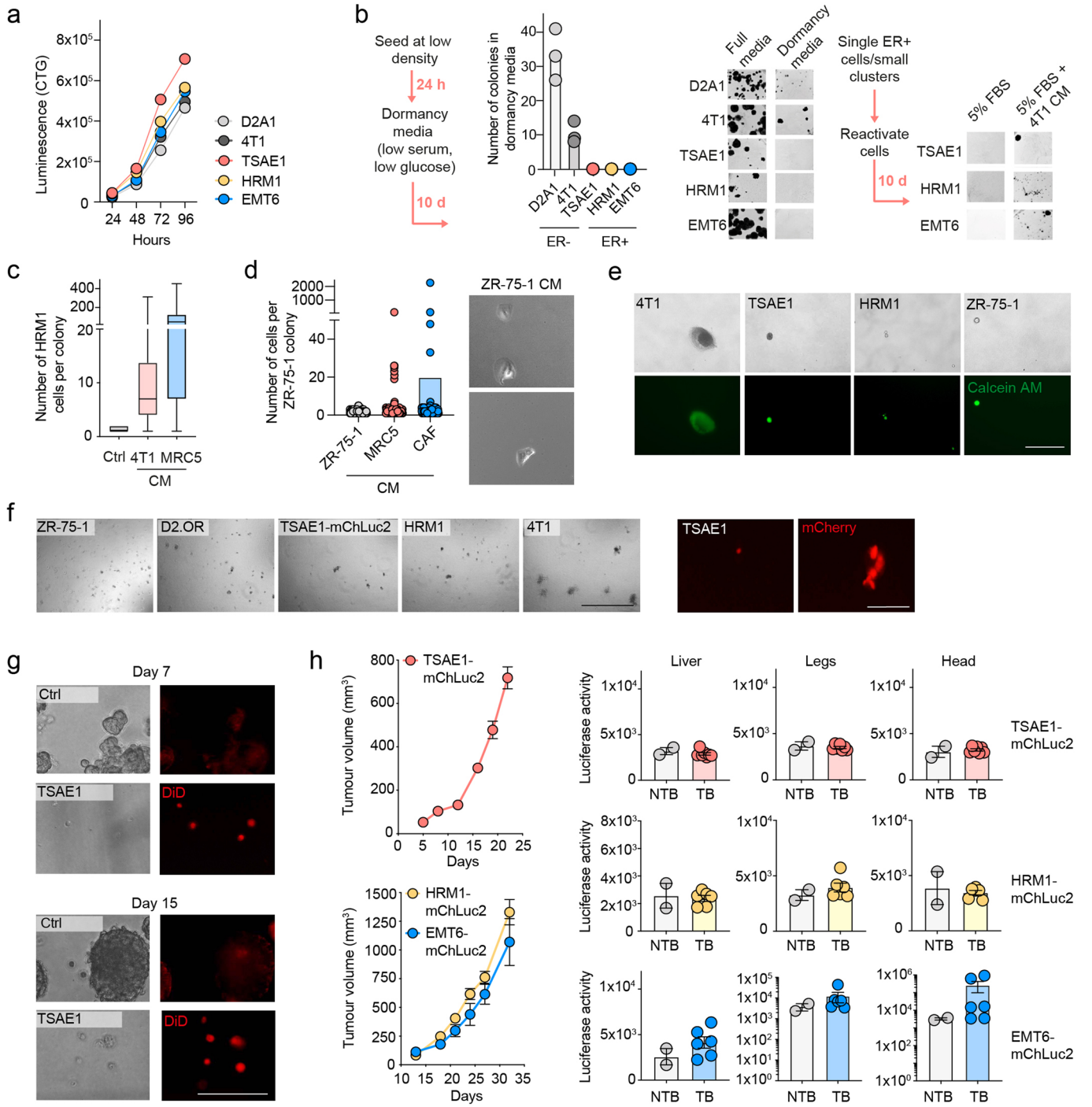

Extended Data Fig. 2 | ER⁺ tumour cells exhibit dormant phenotypes. **a**, CellTiter-Glo (CTG) analysis of D2A1, 4T1, TSAE1, HRM1 and EMT6 cells. **b**, 100 tumour cells per well were seeded in 6-well plates and the following day changed into dormancy media for 10 days. Left, colonies per well (crystal violet staining), with representative images. Right, media was changed to 5% FBS or 4T1 conditioned media (CM) + 5% FBS for a further 10 days for tumour cell reactivation, representative images shown. **c**, Quantification of HRM1 tumour cells per colony following 10 days culture in Ctrl (5% FBS) or 4T1/MRC5 CM with 5% FBS ($n = 10, 51, 35$ colonies, respectively). **d**, 1,000 ZR-75-1 cells per well were seeded in 6-well plates and the following day changed into dormancy media. 7 days later CM was added as indicated for a further 10 days. Quantification of the number of ZR-75-1 cells per colony following reactivation, with representative phase contrast images of dormant ZR-75-1 cells in ZR-75-1 CM shown (scale bar, 200 µm). **e**, 5,000 cells were seeded in a soft agar-coated 6-well plates. Colonies were stained with Calcein AM 6 weeks after seeding. Representative images (scale bar, 200 µm). **f**, Representative images of tumour cells in BME dormancy assays 9 days after seeding. Scale bars; 500 µm (phase contrast), 100 µm (fluorescence). **g**, Representative images of DiD-labelled TSAE1 cells in BME dormancy assays 7 and 15 days after seeding. Ctrl, a proliferating control (higher numbers of tumour cells seeded). Scale bar, 200 µm. **h**, Additional data associated with Fig. 1h. Left, HRM1-mChLuc2, EMT6-mChLuc2 and TSAE1-mChLuc2 primary tumour growth. Right, *ex vivo* IVIS quantification of metastatic spread (total counts) to liver, hind legs and head. NTB, non-tumour bearing control mice; TB, tumour bearing. The same NTB mice were used for HRM1-mChLuc2 and EMT6-mChLuc2. Representative data of three (**a,b,f**) or two (**c,d,g**) independent repeats, with multiple cell lines. Data are presented as mean values; **h**, ±SEM; **c**, box plot shows 25th/75th percentiles, median (line) and minimum/maximum values (whiskers).

https://doi.org/10.1038/s43018-023-00525-y

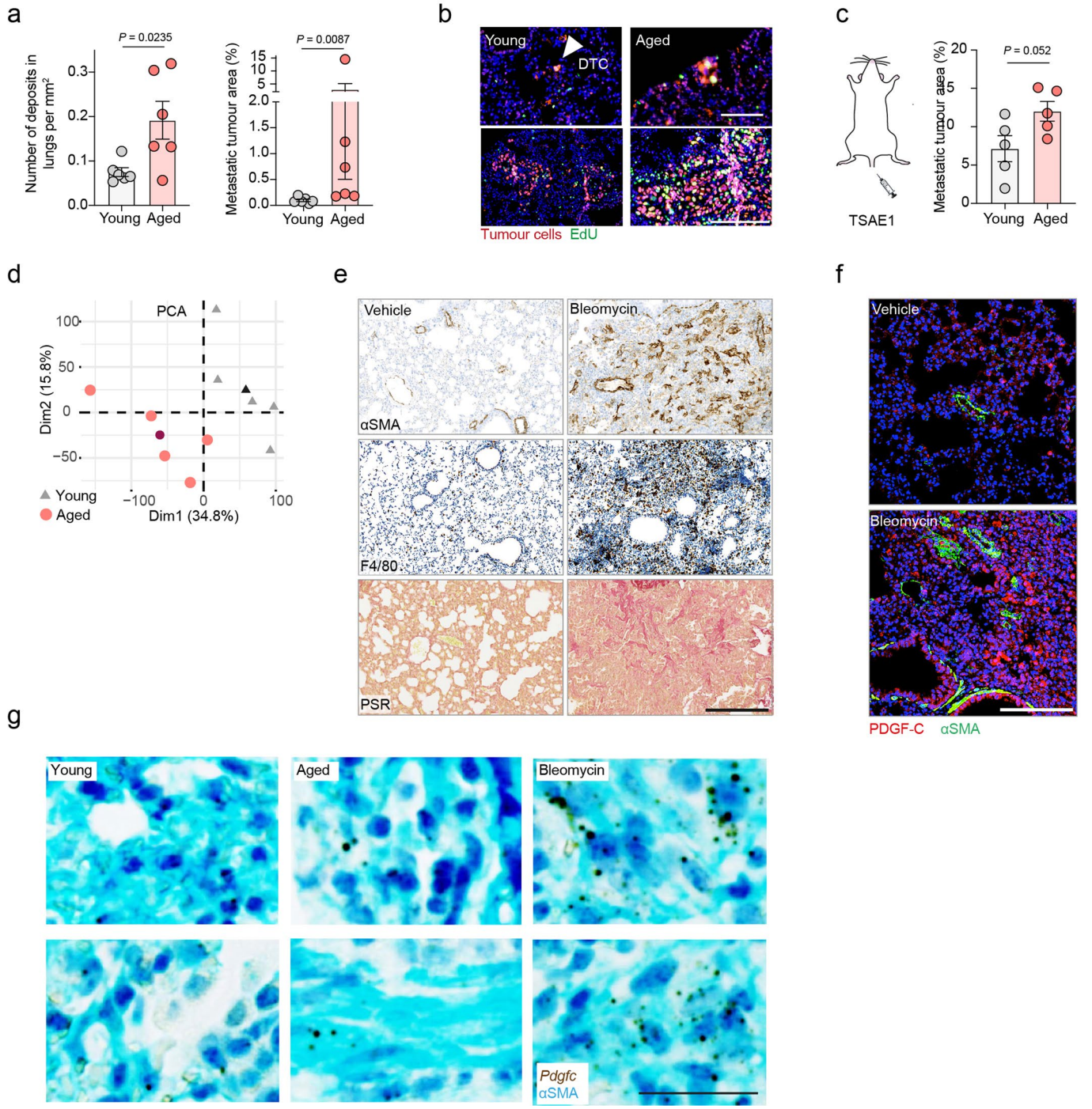

Extended Data Fig. 3 | PDGF-C levels are upregulated in aged and fibrotic lungs. a, Additional quantification for Fig. 2a. Left, number of metastatic deposits in the lungs. Right, percentage metastatic tumour area in the lungs. **b**, Additional images of the experiment presented in Fig. 2b illustrating EdU+ tumour cells in young and aged mouse lungs. Tumour cells were identified by staining with an antibody against HMGA2. White arrowhead points to single dormant tumour cell (scale bars; 100 µm, upper images; 250 µm, lower images). **c**, Independent repeat of the experiment presented in Fig. 2c. TSAE1 tumour cells were injected intravenously into the tail vein of young ($n = 5$ mice) or aged (14-month, $n = 5$ mice) BALB/c mice. Percentage metastatic tumour burden in the lungs (day 15). **d**, Associated with Fig. 2d. Principal component analysis (PCA) of young (grey triangles) and aged (light red circles) NTB mouse lungs (RNA-seq data). Average values per group are shown with black and dark red shapes for young and aged lungs, respectively. **e,f**, BALB/c mice were treated with vehicle or bleomycin (see Methods for schedule) and culled 7 or 14 days after treatment ended ($n = 3$ mice per group). **e**, Representative images of αSMA and F4/80 (7 days post-treatment) and picrosirius red (PSR) (14 days post-treatment) staining in lungs (scale bar, 250 µm). **f**, Representative images of αSMA (green), PDGF-C (red) and DAPI (blue) staining in lungs of mice culled 14 days after treatment ended (scale bar, 150 µm). **g**, RNAscope analysis of *Pdgfc* expression in young (12-week), aged (13-month) or fibrotic (bleomycin-treated) lungs (from experiments shown in Fig. 2d,h). Lung sections were counterstained for αSMA (cyan). Scale bar, 25 µm. **a,c**, Data are presented as mean values ±SEM; **a** (left), **c**, two-tailed *t*-test; **a** (right), two-tailed Mann-Whitney *U*-test.

https://doi.org/10.1038/s43018-023-00525-y

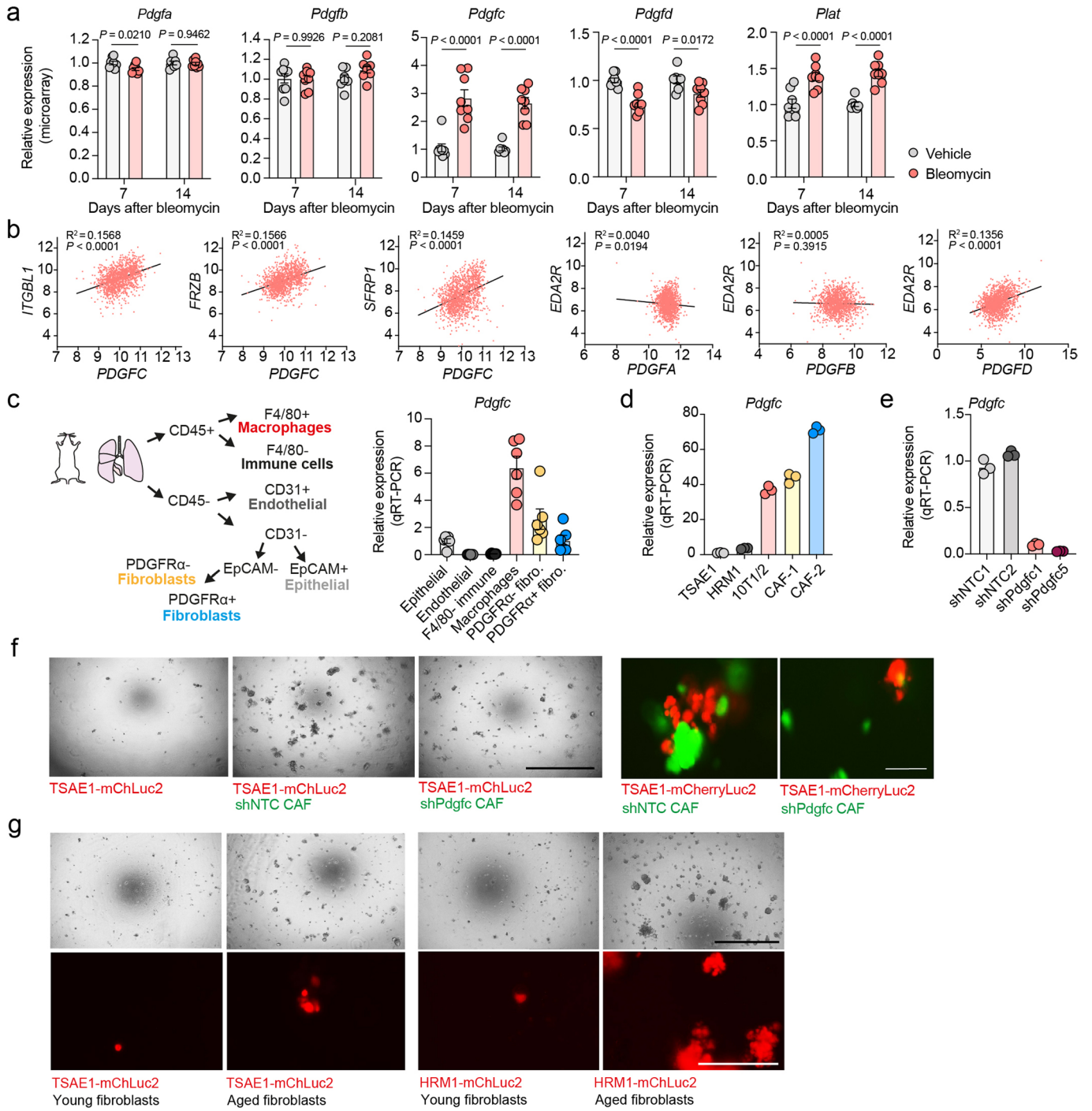

Extended Data Fig. 4 | *Pdgfc*/*PDGFC* expression in the aged microenvironment and its role in release from dormancy. a, Transcriptional profiling of C57BL/6 mouse lungs treated with vehicle or bleomycin (from GSE40151). Analysis of *Pdgfa-d* and *Plat* expression in lungs 7 and 14 days post-treatment, $n = 8$ mice per group except $n = 7$ mice for vehicle 14 days. **b**, Associated with Fig. 2i. Transcriptional profiling of human non-cancerous lung tissues (GSE23546). Correlation of *PDGF* expression and expression of the age-associated genes *EDA2R, ITGBL1, FRZB and SFRP1*[15,17] in lung samples from patients aged 4 – 85 years of age ($n = 1197$ patients). **c**, Expression of *Pdgfc* in the aged (18-month) C57BL/6 mouse lung ($n = 6$ mice, 4 females and 2 males). Lung tissue was dissociated and FACSorted for the following populations: macrophages ($CD45^+$ $F4/80^+$), other immune cells ($CD45^+$ $F4/80^-$), endothelial ($CD45^-$ $CD31^+$), epithelial ($CD45^-$, $CD31^-$, $EpCAM^+$) and $PDGFR\alpha^-$ (cells negative for all markers) and $PDGFR\alpha^+$ fibroblasts. **d**, *Pdgfc* expression in GFP^+ mouse CAFs compared to 10T1/2 fibroblasts and ER^+ mouse tumour cells (RT-qPCR). **e**, GFP^+ mouse CAFs were transduced with two non-targeting control shRNAs (shNTC1, shNTC2) or two independent shRNAs targeting *Pdgfc* (shPdgfc1, shPdgfc5). RT-qPCR to assess *Pdgfc* expression. **f**, TSAE1-mChLuc2 cells were cultured in BME assays (see Extended Data Fig. 2f) for 9 days with or without shNTC or shPdgfc CAFs and then imaged on an EVOS microscope; tumour cells ($mCherry^+$) and CAFs (GFP^+). Scale bar, 1 mm (phase-contrast images) and 100 µm (fluorescent images). **g**, TSAE1-mChLuc2 or HRM1-mChLuc2 cells were cultured in BME assays for 9 days (see Extended Data Fig. 2f) with or without immortalised young or aged mouse lung fibroblasts. Cells were imaged on an EVOS microscope: tumour cells ($mCherry^+$). Scale bar, 1 mm (phase-contrast images) and 200 µm (fluorescent images). **a,c-e**, Data are presented as mean values; **a,c**, ±SEM; **a**, two-way ANOVA; **b**, two-tailed Pearson's correlation (line shows linear regression). **f,g**, Representative of two-independent repeats. **g**, Two independent young and old fibroblast populations were used with equivalent results.

https://doi.org/10.1038/s43018-023-00525-y

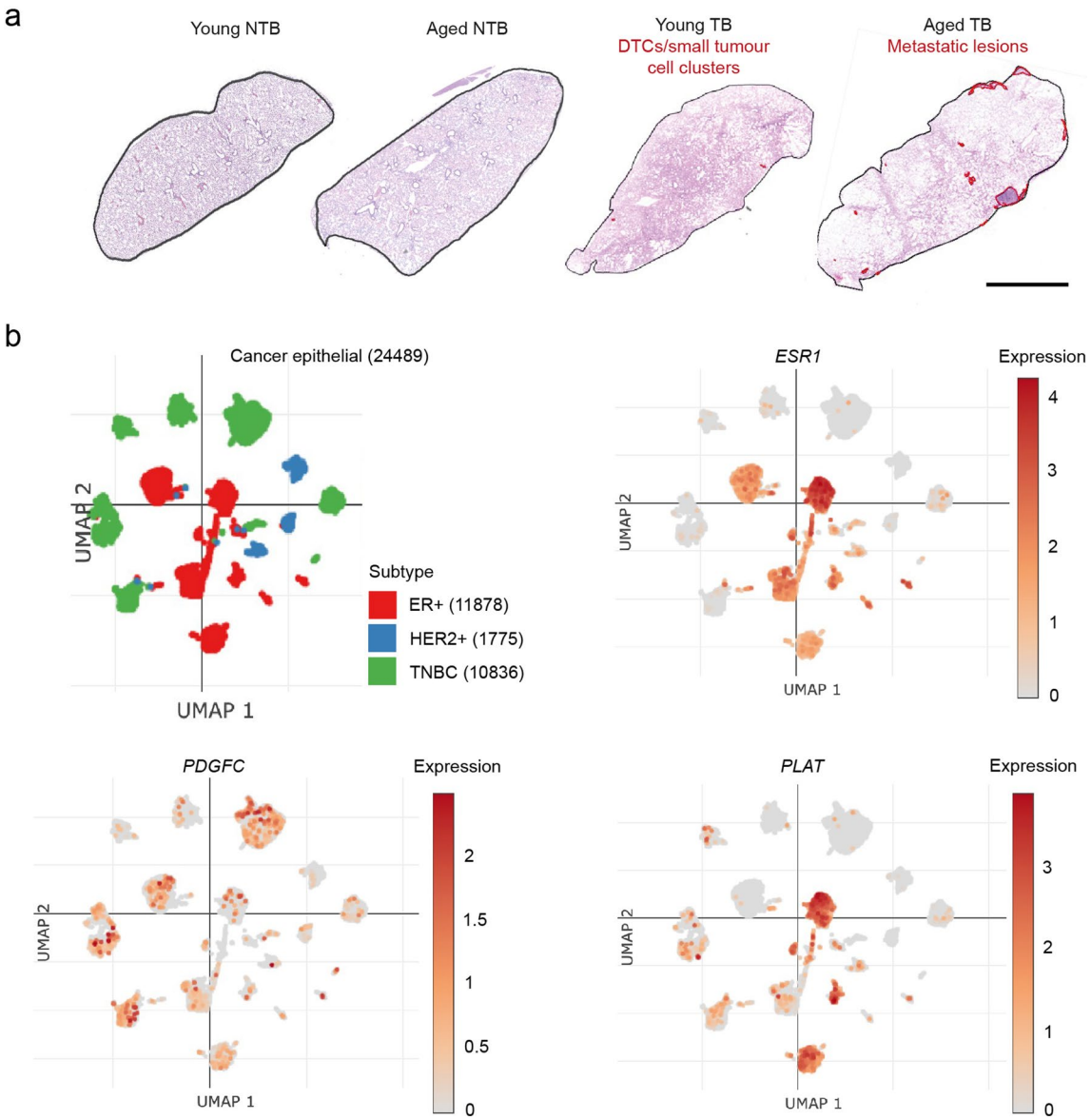

Extended Data Fig. 5 | *PDGFC* expression in human breast cancer cells. **a**, Associated with Fig. 3a,b. Young (12-week) or aged (13-month) BALB/c mice were either left as non-tumour bearing (NTB, $n = 5$ mice per group) or inoculated orthotopically with TSAE1 tumour cells (TB) and culled at day 29 ($n = 7$ young mice, $n = 6$ aged mice). Lungs were divided into the left lobe for histology and the right lobes for RNA-seq analysis. Representative H&E-stained sections of left lung lobes with metastatic deposits outlined in red (scale bar, 5 mm). **b**, Single-cell RNA-seq data from 26 human breast cancers (11 ER^+, 5 $HER2^+$ and 10 TNBC, triple-negative; number of cells sequenced shown in brackets), clustering of epithelial cancer cells based on subtype[21]. Expression of *ESR1*, *PDGFC* and *PLAT* are shown. Plots were generated using the Broad Institute single-cell portal, https://singlecell.broadinstitute.org.

https://doi.org/10.1038/s43018-023-00525-y

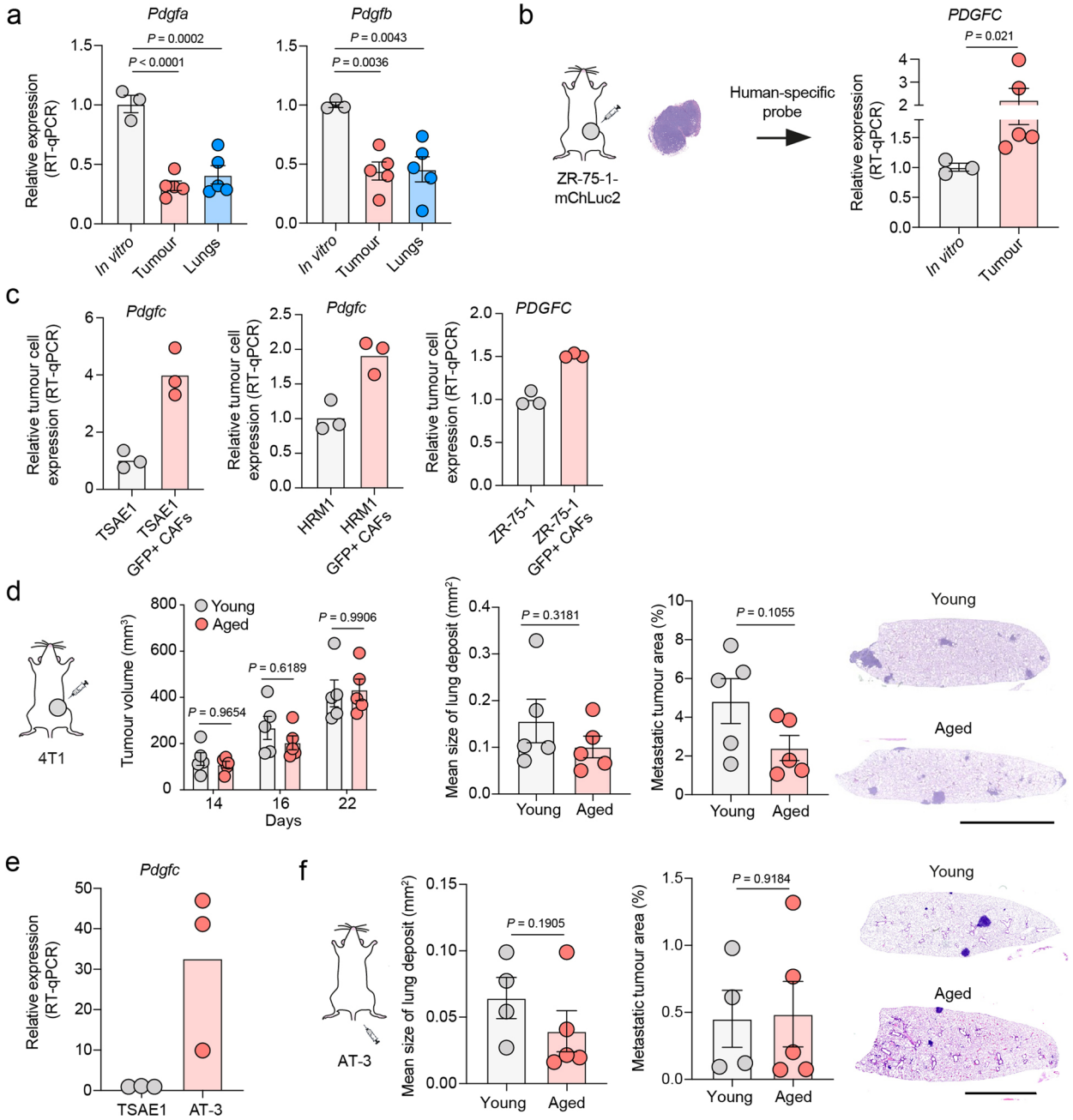

Extended Data Fig. 6 | ER⁻ mouse mammary tumour cells show equivalent metastasis in young and aged mice. a, Additional data associated with Fig. 3g. TSAE1-mChLuc2 cells were isolated from the primary tumours or metastatic lungs, and tumour cell *Pdgfa* and *Pdgfb* expression assessed (RT-qPCR) and compared to expression in *in vitro* cultured cells ($n = 3$ biological repeats). **b**, *PDGFC* expression in ZR-75-1-mChLuc2 cells *in vitro* ($n = 3$ biological repeats) or isolated from primary tumours following orthotopic inoculation into NSG mice. RT-qPCR using a human-specific probe ($n = 5$ mice). **c**, 575,000 GFP⁺ CAFs were seeded with 200,000 TSAE1 or HRM1 tumour cells or 575,000 ZR-75-1 cells in 6-cm dishes in DMEM (10% FBS) and cultured for 48 hours. For monocultures, 400,000 TSAE1 or HRM1 cells or 750,000 ZR-75-1 cells were seeded. Single cell suspensions were stained with DAPI to exclude dead cells. 100,000-200,000 GFP-negative tumour cells were sorted on a Sony SH800 cell sorter and collected for RNA extraction. RT-qPCR analysis of *Pdgfc*/*PDGFC* expression (as detailed in Methods). Representative data of two (ZR-75-1) or three (TSAE1 and HRM1) independent repeats, with two independent CAF populations. **d**, 4T1 cells were inoculated orthotopically into young ($n = 5$ mice) or aged (>12-month, $n = 5$ mice) BALB/c mice. Left, tumour volume. Right, quantification of spontaneous metastasis to the lung, with representative images shown (scale bar, 5 mm). **e**, *Pdgfc* expression (RT-qPCR) in ER⁻ AT-3 cells culture *in vitro* compared to ER⁺ TSAE1 cells. **f**, AT-3 cells were inoculated intravenously into young ($n = 4$ mice) or aged (18-month, $n = 5$ mice) C57BL/6 mice. Quantification of lung metastasis. Data are presented as mean values; **a,b,d,f**, ±SEM; **a**, one-way ANOVA with multiple comparisons; **b,f** (left), two-tailed Mann-Whitney *U*-test; **d** (left), two-way ANOVA with multiple comparisons; **d**, (right), **f** (right), two-tailed *t*-test.

https://doi.org/10.1038/s43018-023-00525-y

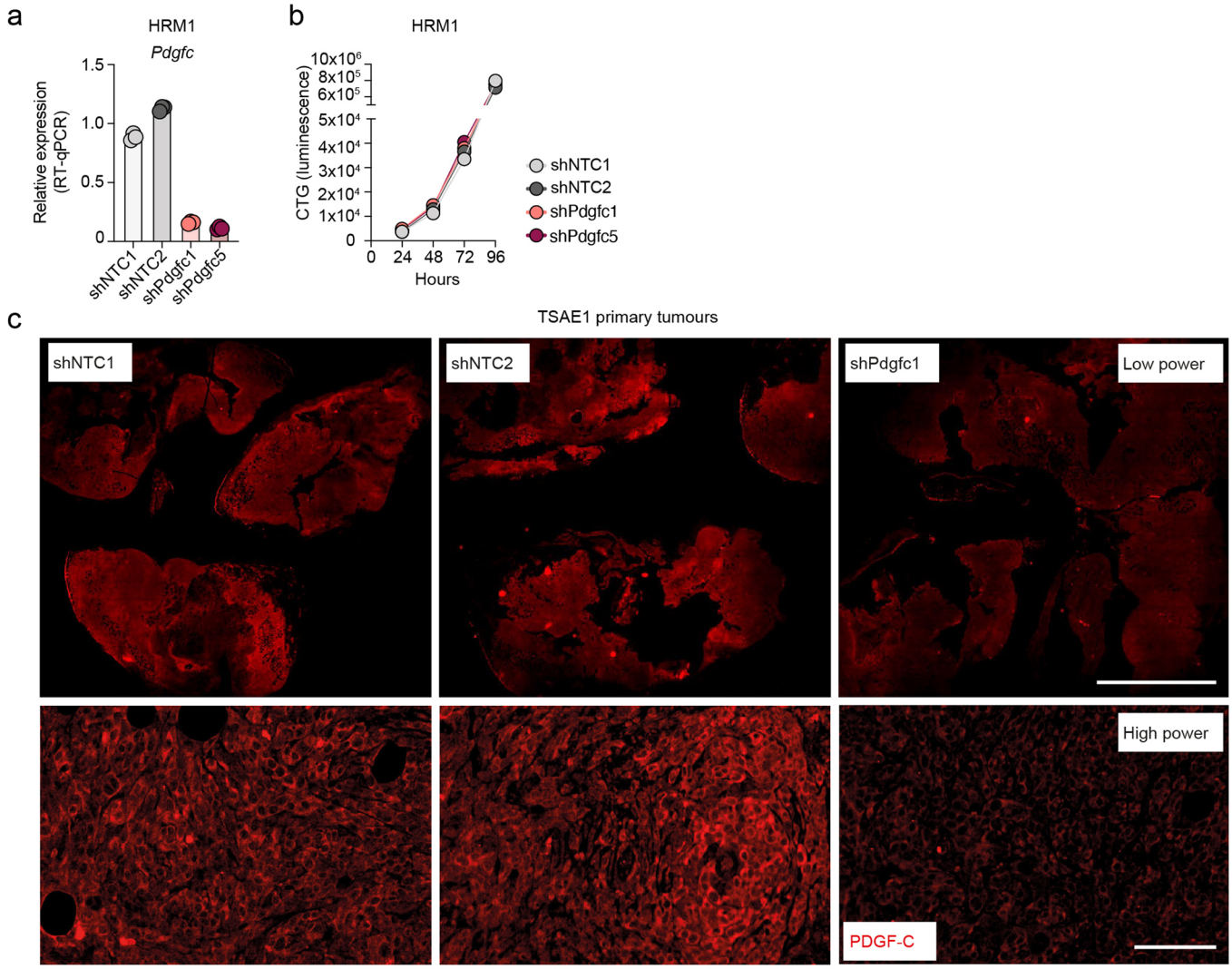

Extended Data Fig. 7 | Validation of *Pdgfc* downregulated expression in HRM1 cells and TSAE1 tumours. a,b, Associated with Fig. 4d. Data are presented as mean values. a, *Pdgfc* expression (RT-qPCR) in HRM1 shNTC (1,2) and shPdgfc (1,5) cells. b, Proliferation of HRM1 shNTC (1,2) and shPdgfc (1,5) cells assessed by CellTiter-Glo (CTG). Representative data of two independent repeats. c, Immunostaining for PDGF-C in TSAE1 shNTC1, shNTC2 and shPdgfc1 primary tumours from Fig. 4f (representative images; scale bar, 5 mm and 250 µm for low- and high-power images, respectively).

https://doi.org/10.1038/s43018-023-00525-y

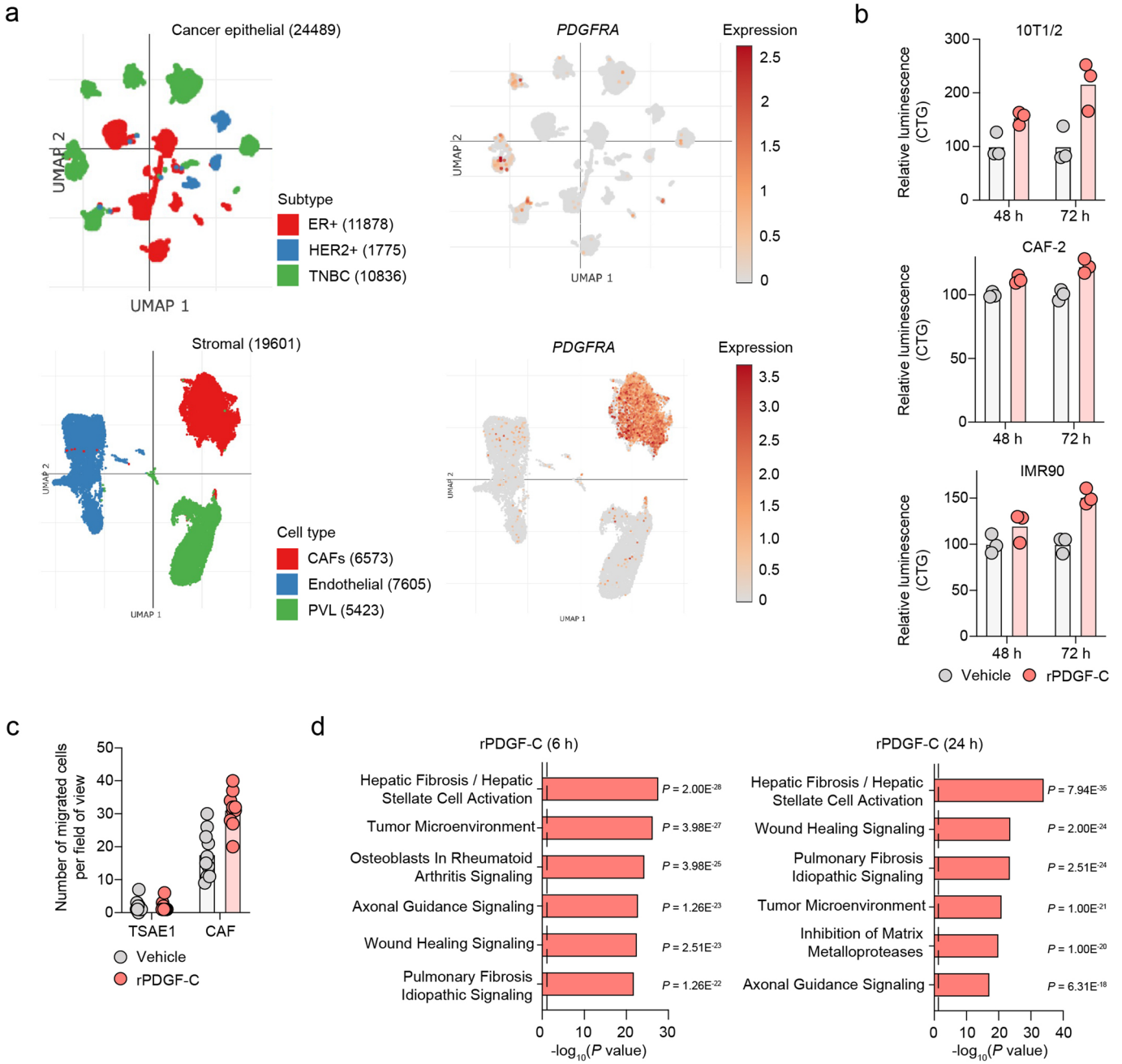

Extended Data Fig. 8 | PDGF-C promotes fibroblast proliferation and migration but has no effect on tumour cells. a, Single-cell RNA-seq data from 26 human breast cancers (11 ER$^+$, 5 HER2$^+$ and 10 TNBC, triple negative)[21]. Expression of *PDGFRA* is shown in cancer and stromal cells. Number of cells sequenced is indicated in brackets. PVL, perivascular-like. Plots were generated using the Broad Institute single-cell portal, https://singlecell.broadinstitute.org. **b**, Additional data associated with Fig. 5c. CellTiter-Glo analysis following vehicle or rPDGF-C treatment (100 ng mL^{-1}) for mouse (upper, middle) and human (lower) fibroblasts. Representative data of two (10T1/2 and CAF-2) or three (IMR90) independent repeats, in multiple cell lines. **c**, Transwell migration assay. Following overnight culture in SFM, 5,000 cells were seeded into Transwell inserts (8.0 µm pore size, Corning 3422) in SFM. DMEM plus 2% FBS containing vehicle or rPDGF-C (100 ng mL^{-1}) was added per well. Treatments were refreshed at 24 hours. After 48 hours, inserts were washed, fixed (4% paraformaldehyde) and stained with DAPI. Non-migrated cells were removed from the top of the insert with a cotton tip. 4-5 images were taken per insert. Data show number of migrated CAF and TSAE1 cells per field of view. Representative data of three independent repeats. **d**, Ingenuity pathway analysis showing the top 6 significantly ($P < 0.05$, right-tailed Fisher's exact test) altered pathways following treatment with rPDGF-C of MRC5 fibroblasts. Dashed line indicates *P* value cut-off. **b,c**, Data are presented as mean values.

https://doi.org/10.1038/s43018-023-00525-y

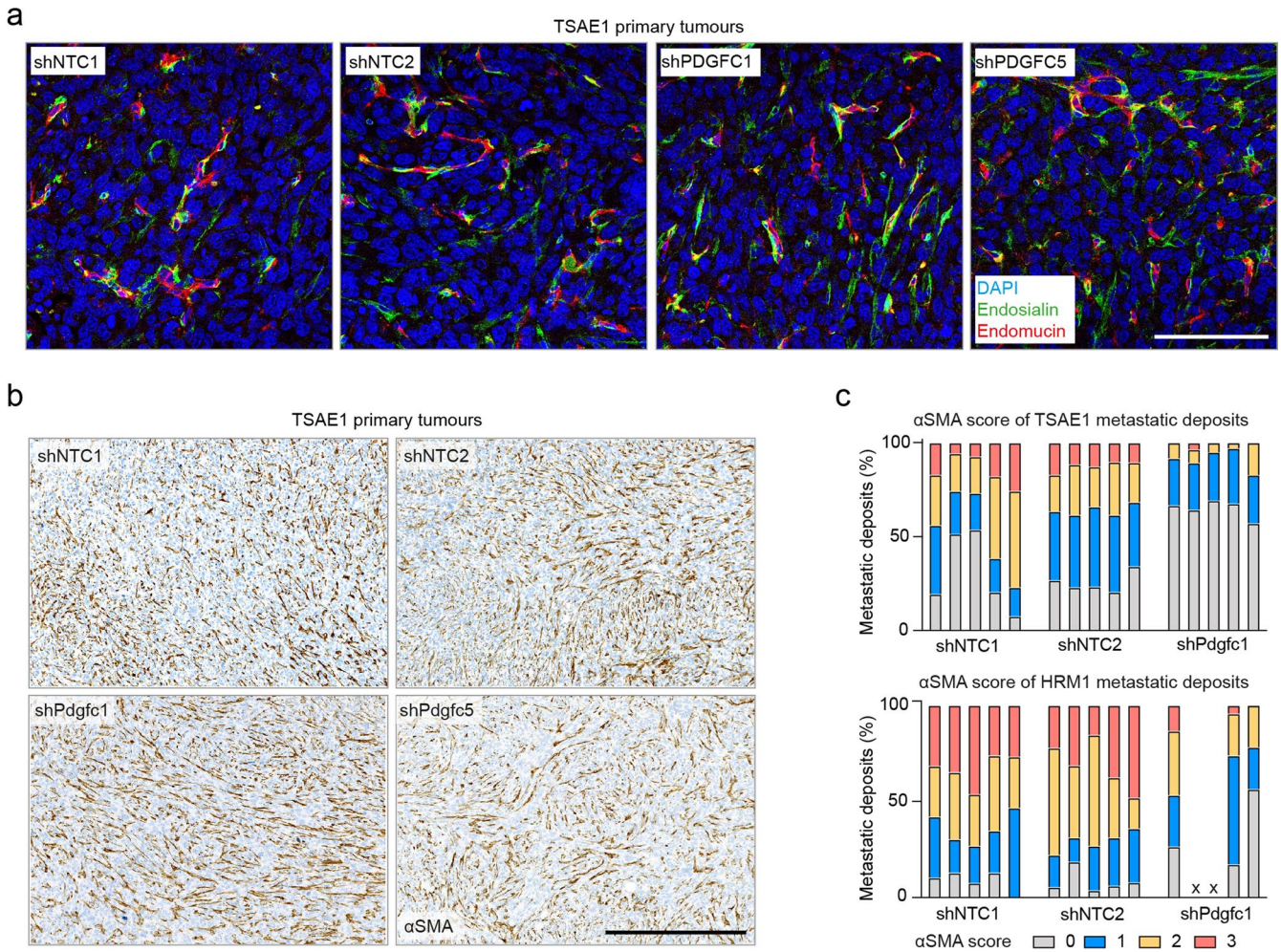

Extended Data Fig. 9 | *Pdgfc* knockdown in tumour cells has limited effects on the primary tumour stroma but reduces αSMA$^+$ CAF numbers in metastatic deposits. a,b, Representative immunostaining of shNTC (1,2) and shPdgfc (1,5) TSAE1 primary tumours from Fig. 4f. **a**, Sections stained for the endothelial marker endomucin (red), pericyte marker endosialin (green) and DAPI (blue) (scale bar, 100 μm). Brightness/contrast adjustment was performed on individual channels (ImageJ; all panels adjusted the same) before merging. **b**, αSMA immunohistochemistry (scale bar, 500 μm). **c**, Scoring of αSMA positivity of the lung metastases from Fig. 5e,f. Each bar represents an individual mouse. Scores calculated based on percentage of the metastatic deposit that was αSMA-positive: 0, 0%; 1, <20%; 2, 20-50%; 3, >50%. Note, two HRM1-shPdgfc mice had no detectable lung deposits, labelled as 'x'.

https://doi.org/10.1038/s43018-023-00525-y

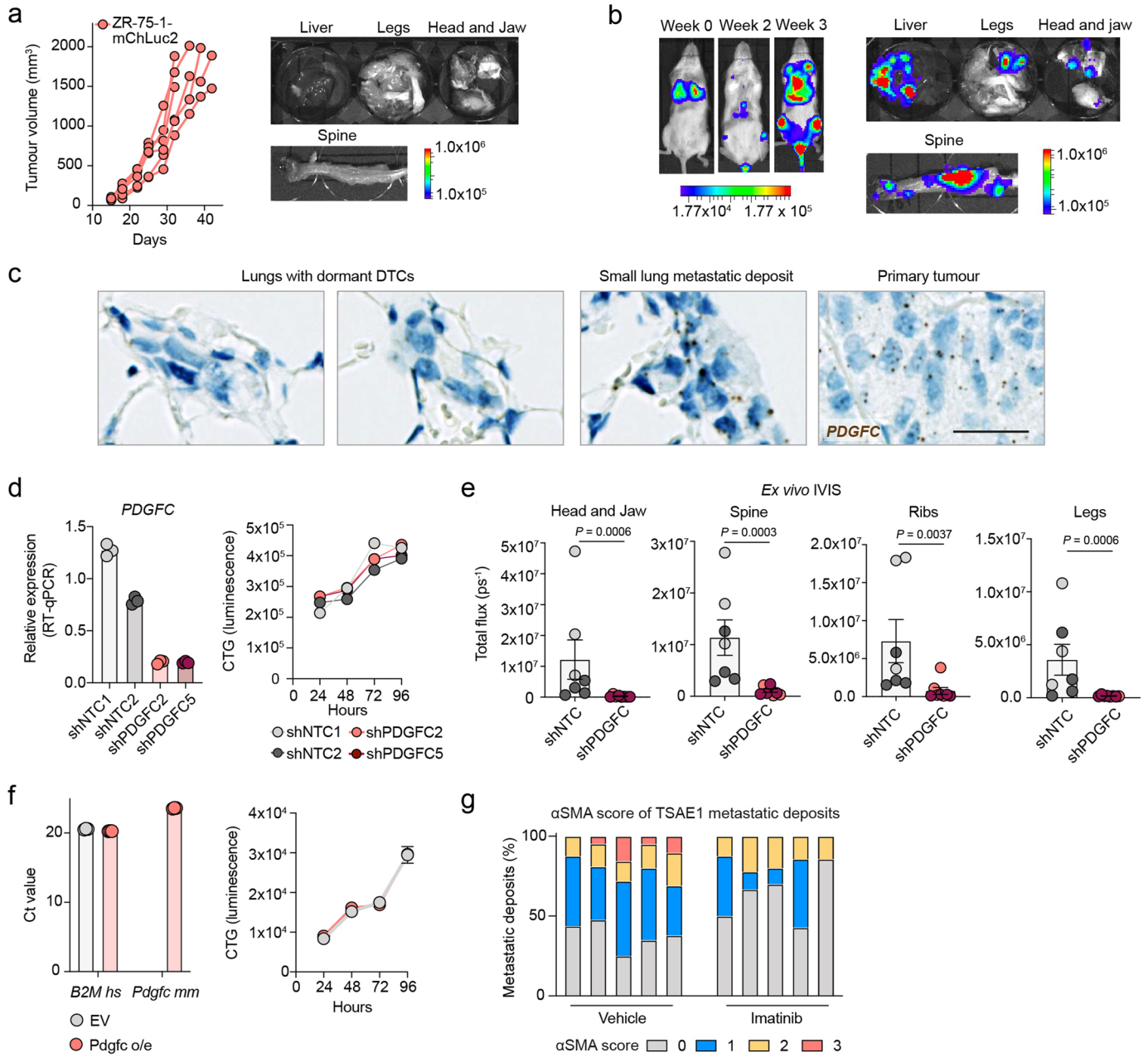

Extended Data Fig. 10 | Metastasis of ZR-75-1 human ER⁺ breast cancer cells and effects of *PDGFC* knockdown or imatinib treatment. a, Additional data associated with Fig. 6a. ZR-75-1-mChLuc2 cells injected orthotopically into $n = 5$ NSG mice. Left, tumour growth of individual mice. Right, representative *ex vivo* IVIS images of organs at endpoint (day 34-43). **b**, Associated with Fig. 6b. ZR-75-1-mChLuc2 cells injected intravenously into $n = 6$ NSG mice. Left, representative whole-body IVIS images of one mouse at week 0 (2 hours after tumour cell inoculation), week 2 and week 3. Right, representative *ex vivo* IVIS images of organs at endpoint (day 29). **c**, *PDGFC* (human-specific) RNAscope analysis of mouse tissue with human ZR-75-1 tumour cells from Fig. 6a,b. Representative images of lungs with dormant DTCs (spontaneous, first panel; experimental metastasis, second panel), a small lung deposit (experimental metastasis) and a primary tumour. Scale bar, 25 µm. **d**, Validation of ZR-75-1 shPDGFC cell lines. Left, *PDGFC* expression (RT-qPCR) in ZR-75-1-mChLuc2 shNTC(1,2) and shPDGFC(2,5) cells cultured *in vitro*. Representative data of two independent repeats. Right, proliferation of ZR-75-1-mChLuc2 shNTC(1,2) and shPDGFC(2,5) cells assessed by CellTiter-Glo (representative data of two independent repeats). **e**, Associated with Fig. 6c. ZR-75-1-mChLuc2 shNTC(1,2) and shPDGFC(2,5) cells injected intravenously in NSG mice (shNTC(1&2) and shPDGFC5(2&5); $n = 7$ or 8 mice per group, respectively). Quantification of *ex vivo* IVIS signal in organs (day 29). Light grey, shNTC1; dark grey, shNTC2; light red, shPDGFC2; dark red, shPDGFC5. **f**, Associated with Fig. 6e. Validation of ZR-75-1 EV and Pdgfc over-expression (o/e) cell lines. Left, Ct values (RT-qPCR) for human (Hs) *B2M* and mouse (Mm) *Pdgfc* (RT-qPCR). Right, proliferation of ZR-75-1 EV and Pdgfc o/e cells assessed by CellTiter-Glo (representative data of three independent repeats). **g**, Scoring of αSMA positivity of lung metastases from Fig. 7b. Each bar represents an individual mouse. Scores calculated based on percentage of the metastatic deposit that was αSMA-positive: 0, 0%; 1, <20%; 2, 20-50%; 3, >50%. d-f, Data represent mean values; e, ±SEM, two-tailed Mann-Whitney *U*-test.

nature portfolio

Corresponding author(s): Clare M. Isacke

Last updated by author(s): 15/1/23

Reporting Summary

Nature Portfolio wishes to improve the reproducibility of the work that we publish. This form provides structure for consistency and transparency in reporting. For further information on Nature Portfolio policies, see our Editorial Policies and the Editorial Policy Checklist.

Statistics

For all statistical analyses, confirm that the following items are present in the figure legend, table legend, main text, or Methods section.

n/a	Confirmed	
☐	☒	The exact sample size (*n*) for each experimental group/condition, given as a discrete number and unit of measurement
☒	☐	A statement on whether measurements were taken from distinct samples or whether the same sample was measured repeatedly
☐	☒	The statistical test(s) used AND whether they are one- or two-sided *Only common tests should be described solely by name; describe more complex techniques in the Methods section.*
☐	☒	A description of all covariates tested
☐	☒	A description of any assumptions or corrections, such as tests of normality and adjustment for multiple comparisons
☐	☒	A full description of the statistical parameters including central tendency (e.g. means) or other basic estimates (e.g. regression coefficient) AND variation (e.g. standard deviation) or associated estimates of uncertainty (e.g. confidence intervals)
☐	☒	For null hypothesis testing, the test statistic (e.g. *F*, *t*, *r*) with confidence intervals, effect sizes, degrees of freedom and *P* value noted *Give P values as exact values whenever suitable.*
☒	☐	For Bayesian analysis, information on the choice of priors and Markov chain Monte Carlo settings
☒	☐	For hierarchical and complex designs, identification of the appropriate level for tests and full reporting of outcomes
☐	☒	Estimates of effect sizes (e.g. Cohen's *d*, Pearson's *r*), indicating how they were calculated

Our web collection on statistics for biologists contains articles on many of the points above.

Software and code

Policy information about availability of computer code

Data collection	No software was used for data collection.
Data analysis	GraphPad Prism (8.4.3), Fiji (Image J; 2.0.0-rc-54/1.51h), Living image software (PerkinElmer,4.7.3), QuantStudio Real-Time PCR Software (1.7.1), NDP.view2 (2.7.52), Image Lab (Bio-rad, 6.1), SH800 and BD FACSDiva (8.0.1) software, Ventana Discovery Ultra (VSS v12.5.4). For analysis of RNA-seq data: FastQC (v0.11.4), and as previously described (Jungwirth et al. 2021 Nat. Commun.). For human fibroblast RNA-seq, trim-galore v0.6.6, GRCh38 using STAR aligner v2.7.6a, R package edgeR's (v3.28.1) TMM method in R statistical programming environment (v3.6.0). Gene Set Enrichment Analysis (GSEA 4.1.0), Ingenuity pathway analysis (version 01-20-04), heatmaps generated on MeV (4.8.1), R packages FactoMineR_(v2.4) and factoextra_(v1.0.7) for principal component analysis.

For manuscripts utilizing custom algorithms or software that are central to the research but not yet described in published literature, software must be made available to editors and reviewers. We strongly encourage code deposition in a community repository (e.g. GitHub). See the Nature Portfolio guidelines for submitting code & software for further information.

Data

Policy information about availability of data

All manuscripts must include a data availability statement. This statement should provide the following information, where applicable:

- Accession codes, unique identifiers, or web links for publicly available datasets
- A description of any restrictions on data availability
- For clinical datasets or third party data, please ensure that the statement adheres to our policy

The RNA-seq datasets (Fig1-3) are deposited in the Sequence Read Archive (SRA) under the accession number PRJNA822368. The data for the human fibroblast

RNA-seq (Fig 5) is deposited in SRA (PRJNA895434). METABRIC dataset were downloaded from cBioportal. Expression data for human breast cancer cell lines were downloaded from the Broad Institute (CCLE). Non-cancerous lung gene expression data (GSE23546) and gene expression data for C57BL/6 mice treated with bleomycin (GSE40151) were downloaded from GEO. Details of publicly available datasets analysed, and references to the original publications, are also included in the section 'Human data set analysis'.

Field-specific reporting

Please select the one below that is the best fit for your research. If you are not sure, read the appropriate sections before making your selection.

☒ Life sciences ☐ Behavioural & social sciences ☐ Ecological, evolutionary & environmental sciences

For a reference copy of the document with all sections, see nature.com/documents/nr-reporting-summary-flat.pdf

Life sciences study design

All studies must disclose on these points even when the disclosure is negative.

Sample size	Sample sizes for in vivo metastasis experiments were between 4 and 8 mice per group which was based on laboratory experience (Jungwirth et al. 2021 Nat. Commun; Jungwirth et al. 2018 DMM; Jenkins et al. 2022). One exception was N=3 D2A1 tumours for Pdgfc expression (Fig. 3h) due to mouse availability. For the experiment with non-tumour bearing mice used to assess expression (RT-qPCR) following vehicle/ bleomycin treatment (Fig. 2h) N=3 per group was considered sufficient for analysis of expression in the naive lung due to the absence of variability in tumour growth. For syngeneic spontaneous metastasis assays we used 6 mice per group (a minimum of 5 for xenograft experiments) due to the variability in primary tumour growth and thus increased variability/ higher standard deviations. Exceptions to this were Fig 2b (EdU analysis; N=4 young, N=3 aged) where groups where matched for primary tumour size. For in vitro studies, a minimum of triplicates was used. In vitro sample sizes were chosen based on previous experience for such experiments (Jungwirth et al. 2021 Nat. Commu;Jungwirth et al. 2018 DMM).
Data exclusions	Fig. 4h, one mouse (TSAE1-Pdgfc o/e) did not develop a tumour due to a failed injection and therefore was excluded from the metastasis analysis. Fig. 6c, one mouse (shNTC1) died under anaesthesia during imaging before the experiment endpoint. Fig. 8c, one mouse in aged anti-PDGF-C group due to failed injection. A statistical outlier was identified in Fig 8b (outlier analysis on GraphPad Prism (ROUT, q = 1%)) but was highlighted on the graph and P-values with and without outlier are indicated.
Replication	Animal experiments were repeated on at least one additional occasion with equivalent results except experiments shown in Fig. 1f, Fig. 2b,f,k, Fig. 3g-i, Fig. 4d,e,h, Fig. 6c-e, Fig. 7d, Fig. 8a-c, Extended Data Fig. 1f, Extended Data Fig. 6b,d,f, which were performed once. Fig. 1f was repeated with a second model (Extended Data Fig. 1f); Fig. 2b, metastasis phenotype was seen in other experiments, the EdU was just performed once due to availability of aged mice; Fig. 2f, similar results were observed in experimental metastasis assays (Fig. 2c); Fig. 2k and was performed with two independent controls/shRNAs; Fig. 3g, similar results were observed in a second model (Extended Data Fig. 6b) and findings were validated by RNAScope analysis (Fig. 3f); Fig. 3h and Extended Data Fig. 6d,f were performed with two ER- lines; Fig. 3i, findings were validated by RNAScope analysis (Fig. 3f) and metastatic burden quantification of other experiments (Fig. 2a, Extended Data Fig 3a); Fig. 4d was validation in a second model; Fig. 4h and 6e was validation of a phenotype observed with knockdown; Fig. 6c, was validated in a second model and performed using two independent shRNAs; Fig 7d, Pdgfc knock-down and imatinib (in controls) findings had been seen in a independent experiment only the shPdgfc + imatinib arm was performed once; Fig. 8a,b, are two independent ways of inhibiting PDGFC pathway with similar results observed. Of the remaining in vivo experiments performed only once (Fig. 4e, 6d, Fig. 7b (shPdgfc + imatinib arm) and 8c), Fig. 8c was due to lack of availability of aged mice, Fig. 4e, Fig. 6d, Fig. 7b (shPdgfc + imatinib arm) provide additional data to help support main findings of the paper and had sufficient biological repeats (mice) in the experiment to perform statistical analysis . All in vitro experiments were repeated on at least one additional occasion with equivalent results and/or validated with different cell lines.
Randomization	In all animal experiments mice were randomized based on individual mouse body weights at the start of the experiment apart from Fig. 2b where mice were matched for primary tumour size. For in vitro studies, no randomization was performed as cell lines used in this study were from a single preparation with no reason to believe that the spacial location in the plates/wells affected results.
Blinding	The investigators were not blinded for the allocation of groups during experiments or during in vitro or in vivo experiments as the samples or animals were marked and the same investigator set-up and performed the experiment. Fully blinded animal experiments were not possible due to personnel availability to accommodate such situations. For imaging studies investigators were not blinded during data collection as the same investigator set up and imaged the experiment but all imaging analysis and quantification was performed blinded.

Reporting for specific materials, systems and methods

We require information from authors about some types of materials, experimental systems and methods used in many studies. Here, indicate whether each material, system or method listed is relevant to your study. If you are not sure if a list item applies to your research, read the appropriate section before selecting a response.

Materials & experimental systems

n/a	Involved in the study
☐	☒ Antibodies
☐	☒ Eukaryotic cell lines
☒	☐ Palaeontology and archaeology
☐	☒ Animals and other organisms
☒	☐ Human research participants
☒	☐ Clinical data
☒	☐ Dual use research of concern

Methods

n/a	Involved in the study
☒	☐ ChIP-seq
☐	☒ Flow cytometry
☒	☐ MRI-based neuroimaging

Antibodies

Antibodies used

Information on the antibodies used are provided in Supplementary Table 1 (copied below).

Anti-mouse CD16/CD31 (Fc receptor block) 14-0161-82 eBioscience 1:100 FACS
CD140a APA5 (BV605 conjugated) 135916 BioLegend 1:200 FACS
CD31 390 (BV711 conjugated) 102449 BioLegend 1:400 FACS
CD326 G8.8 (APC/Cy7 conjugated) 118218 BioLegend 1:250 FACS
CD45 30-F11 (PE Cy7 conjugated) 103114 BioLegend 1:500 FACS
F4/80 Cl:A3-1 (AF647 conjugated) MCA497A647 Bio-Rad 1:100 FACS

Actin (Smooth Muscle) (1A4) A2547 Sigma 1:5,000 IF
Endomucin (V7C7) sc-65495 Santa Cruz 1:1,000 IF
Endosialin (P13) - In-house 1:500 IF
HMGA2 PA521320 Thermo Fisher Scientific 1:300 IF
Lamin A + Lamin C [EPR4100] ab108595 Abcam 1:1,000 IF
PDGF-C TA351509 Origene 1:100 IF
Goat-anti-Mouse-IgG2a-488 A21131 Thermo Fisher Scientific 1:1,000 IF
Goat-anti-Rabbit-Ig-488 A11134 Thermo Fisher Scientific 1:1,000 IF
Goat-anti-Rabbit-Ig-555 A21429 Thermo Fisher Scientific 1:1,000 IF
Goat-anti-Rat-555 A21434 Thermo Fisher Scientific 1:1,000 IF

Actin (Smooth Muscle) (1A4) M0851 Agilent DAKO 1:800 IHC
Actin (Smooth Muscle) (1A4) M0851 Agilent DAKO 1:1,600 IHC + ISH
ERalpha 6F11 NCL-L-ER-6F11 Leica Biosystems 1:40 IHC
F4/80 Cl:A3-1 MCA497 Bio-Rad 1:100 IHC
Firefly luciferase ab181640 Abcam 1:100 IHC
Lamin A + Lamin C (human) [EPR4100] ab108595 Abcam 1:750 IHC

PDGF-C AF1447 Bio-Techne 20 ug In vivo
Goat IgG control AB-108-C Bio-Techne 20 ug In vivo

Akt 9272 Cell Signaling 1:1,000 WB
p44/42 MAPK (Erk1/2) (137F5) 4695 Cell Signaling 1:1,000 WB
PDGF Receptor α (D1E1E) XP 3174 Cell Signaling 1:1,000 WB
Phospho-p44/42 MAPK (Erk1/2) (Thr202/Tyr204) (D13.14.4E) XP 4370 Cell Signaling 1:2,000 WB
Phospho-Akt (Ser473) 9271 Cell Signaling 1:1,000 WB
Phospho-PDGF Receptor α (Tyr 754) 441008G Thermo Fisher Scientific 1:1,000 WB
Phospho-S6 Ribosomal Protein (Ser235/236) (D57.2.2E) XP 4858 Cell Signaling 1:2,000 WB
S6 Ribosomal Protein (5G10) 2217 Cell Signaling 1:1,000 WB
Vinculin [EPR20407] ab219649 Abcam 1:1,000 WB
Goat anti-Rabbit IgG (H+L)-HRP ab205718 Abcam 1:10,000 WB

FACS, Fluorescence activated cell sorting; IF, immunofluorescence; IHC, immunohistochemistry; ISH, in situ hybridisation; WB, Western blotting

Validation

Antibodies were obtained commercially and were validated by the manufacturer (see validation statements below) apart from P13 (Endosialin) that was made in-house and was validated by staining of MCF7 cells transfected with vector or endosialin (MacFadyen, 2007, GEP), with additionally no staining observed in FFPE tissue from Endosialin KO mice; antibodies for IHC were verified in-house by Breast Cancer Now Toby Robins Research Centre Nina Barough Pathology Core Facility using a panel of human and mouse tissues positive and negative for the target (for the luciferase antibody lungs 1.5h after iv injection of TSAE1-mChLuc2 or TSAE1-untagged cells were used as positive or negative controls, respectively).

Company validation statements:

Abcam: 'How we validate our antibodies: a closer look at the standards we use in the validation of our antibodies.

Here you will find more information on what is carried out during our application-specific validation processes' ... (see https://www.abcam.com/primary-antibodies/how-we-validate-our-antibodies).

Agilent DAKO: https://www.agilent.com/en/product/immunohistochemistry/antibodies-controls/primary-antibodies/actin-%28smooth-muscle%29-%28concentrate%29-76542

BioLegend: 'All of our products undergo industry-leading rigorous quality control (QC) testing to ensure the highest level of performance and reproducible results. Each lot is compared to an internally established "gold standard" to maintain lot-to-lot consistency. We also conduct wide-scale stability studies to guarantee an accurate shelf-life for our products. Additionally, we test the majority of our products on endogenous cells rather than transfected or immortal cells that may overexpress the analyte...' (see https://www.biolegend.com/en-us/quality/quality-control).

Bio-rad: 'Bio-Rad conducts rigorous in-house testing to guarantee that our antibodies meet our internal benchmarks and perform in their designated applications as expected. Our stringent quality control process is recognized by ISO9001:2015 certification at our manufacturing sites in Kidlington, Oxfordshire, UK, and Puchheim, Germany' (see https://www.bio-rad-antibodies.com/our-antibody-validation-principles.html?JSESSIONID_STERLING=F5A79FCF95CD46E21344A26EBA92A8BC.ecommerce1&evCntryLang=UK-en&EU_COOKIE_PREFS=000&cntry=UK&thirdPartyCookieEnabled=true).

Bio-techne: 'Our R&D Systems brand has been the leading antibody manufacturer for the past 30 years, using the best production standards and quality control specifications in the industry to develop antibodies scientists trust to exhibit high specificity and perform consistently every time. In addition to our established validation procedures, we also implement the 5 Pillars of Antibody Validation...' (see https://www.bio-techne.com/reagents/antibodies/antibody-validation).

Cell Signaling: 'To ensure product performance, we validate all of our antibodies, in-house, in multiple research applications' (see https://www.cellsignal.co.uk/about-us/our-approach-process/cst-antibody-performance-guarantee).

Invitrogen (ThermoScientific, eBioSciences): 'Invitrogen antibodies are currently undergoing a rigorous two-part testing approach Part 1—Target specificity verification - This helps ensure the antibody will bind to the correct target. Our antibodies are being tested using at least one of the following methods to ensure proper functionality in researcher's experiments'... (see https://www.thermofisher.com/uk/en/home/life-science/antibodies/invitrogen-antibody-validation.html)

Leica: https://shop.leicabiosystems.com/en-gb/pid-ER-6F11-L-CE_gl=1*7upcfo*_ga*MTU4OTE2NzQ2Mi4xNjczODUwMzEy*_ga_10W45KVS7Z*MTY3Mzg3NDE0OC4yLjEuMTY3Mzg3NDY5OS4wLjAuMA..

Origene: 'Specificity is one of the most important attributes of antibodies. At OriGene, we have been working hard to validate specificities of our antibodies. Validation Methods: Predicted band detected in Western blot analysis; Independent antibody strategies; 10k protein chip; Western blot using Knockout cell lysates...' (see https://www.origene.com/products/antibodies/quality).

Santa Cruz: ' Primary antibodies directed to mammalian target proteins have been characterized for reactivity against mouse, rat and human proteins' (see https://www.scbt.com/p/endomucin-antibody-v-7c7?gclid=Cj0KCQiAiJSeBhCCARIsAHnAzT8RJNnzQgHgQKPuiyzeqBbJPcvyGTMmxij1mVp7Qvic7Xu8VGRWt0waAnNXEALw_wcB)

Sigma: 'Delivering high-quality antibodies requires us to perform rigorous specificity and sensitivity testing in order to provide our customers with reliable tools that generate consistent results. We routinely perform standard validation processes across our antibody portfolio. Our standard antibody validation processes include verification for each recommended immunodetection application. Each of the thousands of antibodies in our portfolio are certified through our standard validation process to ensure quality and reproducibility' (see https://www.sigmaaldrich.com/GB/en/products/protein-biology/antibodies/enhanced-validation-ab)

Eukaryotic cell lines

Policy information about cell lines

Cell line source(s)	TSAE1 (TS/A-E1), HRM1, EMT6 and F311 cells were provided by Lalage Wakefield with permission from the scientists (Carla De Giovanni, Jean Zhao, Sara Rockwell and Daniel Alonso, respectively) that developed the cell lines. D2A1 and D2OR cells were from Ann Chambers laboratory stocks. D2A1-m1 and D2A1-m2 metastatic sublines were generated previously (Jungwirth et al. 2018 DDM). ZR-75-1, 10T1/2, 3T3, IMR90, 4T1 and HEK293T cells were from ATCC. AT-3 cells were provided by Christophe Paget and Daphnée Soulard (Institute Pasteur de Lille) and were originally from the lab that isolated them (Stewart et al, 2007 and 2009, J Immunol.). GFP-positive-CAFs were generated previously from 4T1-tumour-bearing BALB/c Ub-GFP mice (Jungwirth et al., 2021; Jungwirth et al. 2021 Nat. Commun). Young (BALB-5013 and C57-6013) and aged (A57-6013, two independent batches from 58-78 week-old mice) mouse primary lung fibroblasts were from Cell Biologics. GFP positive-CAFs were generated previously from 4T1-tumour-bearing BALB/c Ub-GFP mice.
Authentication	Human cell lines were tested using short tandem repeat.
Mycoplasma contamination	Cells were routinely tested for mycoplasma and tested negative.
Commonly misidentified lines (See ICLAC register)	No commonly misidentified cell lines were used in the study.

Animals and other organisms

Policy information about studies involving animals; ARRIVE guidelines recommended for reporting animal research

Laboratory animals	6-8 week-old female BALB/c, FVB, C57BL/6 and NSG mice were purchased from Charles River. The aged mice were aged in-house or purchased from Charles River.
Wild animals	No wild animals were used in this study.
Field-collected samples	No field-collected samples were used in this study.
Ethics oversight	All animal work was carried out under UK Home Office Project Licence P6AB1448A and PP4856884(Establishment Licence X702B0E74) granted under the Animals (Scientific Procedures) Act 1986 and approved by the 'Animal Welfare and Ethical Review Body' at the Institute of Cancer Research (ICR) and Imperial College. For primary tumour experiments the maximum tumour size permitted by the licence (mean diameter 18 mm) was not breached. Primary tumour growth data is included in the source data file.

Note that full information on the approval of the study protocol must also be provided in the manuscript.

Flow Cytometry

Plots

Confirm that:

☒ The axis labels state the marker and fluorochrome used (e.g. CD4-FITC).

☒ The axis scales are clearly visible. Include numbers along axes only for bottom left plot of group (a 'group' is an analysis of identical markers).

☒ All plots are contour plots with outliers or pseudocolor plots.

☒ A numerical value for number of cells or percentage (with statistics) is provided.

Methodology

Sample preparation	For the generation of mChLuc2 cell lines, mCherry+ tumour cells were sorted two-three passages after viral transduction on a FACS ARIA III cell sorter. For sorting of CAF-tumour cell co-cultures, cells were collected after 48h and sorted on a Sony SH800. For tissues: lungs and tumours were dissociated with the mouse tumour dissociation or lung dissociation kit (Miltenyi Biotec; 130-096-730 or 130-095-927), collected in Buffer S and dissociated into single cell suspensions using the gentleMACS Octo Dissociator (Miltenyi) using programme 37C_m_TDK_2 or 37C_m_LDK_1, respectively. Red blood cell lysis was performed (BD Biosciences, 555899) followed by an FC block (Thermofisher Scientific, 14-0161-85). Single cells were stained for CD45, CD31, EpCAM, PDGFRα and F4/80 and DAPI for sorting of the different populations (Extended Data Fig. 4c), or CD45, CD31 and DAPI for enable exclusion of immune cells, endothelial cells and dead cells (sorting mCherry+ tumour cells). respectively. Cells from tissues were sorted on a FACS ARIA III cell sorter or a Symphony S6 cell sorter.
Instrument	Sony SH800 cell sorter, FACS ARIA III or a Symphony S6 cell sorter.
Software	SH800 and BD FACSDiva (8.0.1) or (9.5) software.
Cell population abundance	A purity check was routinely performed with purity >80%.
Gating strategy	Samples were first gated to exclude cellular debris (FSC-A/SSC-A) and then SSC-H/SSC-W and FSC-H/FSC-W or SSC-A/SSC-W and FSC-A/FSC-H to discriminate doublets. DAPI was used to identify the live cell population for sorting of in vivo samples. The gate for mCherry was set based on positive and negative controls (tagged and untagged cells growing in vitro, respectively) and the gate for GFP set based on the monocultures (GFP+ CAFs, GFP- tumour cells). For sorting the cell populations from the lungs: CD45+ F4/80- (F4/80- immune cells), CD45+ F4/80+ (macrophages), CD45-CD31+ (endothelial), CD45-CD31-EpCAM+ (epithelial), CD45-CD31-EpCAM-PDGFRA- (PDGFRA- fibroblasts), CD45-CD31-EpCAM-PDGFRA+ (PDGFRA + fibroblasts) (Extended Data Fig. 4c) or CD45-CD31-mCherry positive for the sorting of tumour cells (Fig 3k). Examples of the gating strategies are shown in the Supplementary Information file.

☒ Tick this box to confirm that a figure exemplifying the gating strategy is provided in the Supplementary Information.